

Top-Quark Charge Asymmetry with a Jet Handle

STEFAN BERGE^a AND SUSANNE WESTHOFF^{a,b}

^a *PRISMA Cluster of Excellence, Institut für Physik (WA THEP),
Johannes Gutenberg-Universität, D-55099 Mainz, Germany*

^b *Helmholtz-Institut Mainz, Johannes Gutenberg-Universität
D-55099 Mainz, Germany*

Abstract

Pairs of top and antitop quarks are produced at the LHC to a large extent in association with a hard jet. We investigate the charge asymmetry in $t\bar{t} + j$ production in quantum chromodynamics (QCD) and with additional massive color-octet vector bosons. The total charge asymmetry at the LHC is suppressed by the large charge-symmetric background from gluon-gluon fusion. We show to what extent the asymmetry can be enhanced by suitable phase space cuts and, in particular, elaborate on the kinematics of the hard jet in the $t\bar{t} + j$ final state. We demonstrate that in QCD, the asymmetry amounts to 1.5 % for central jets without an excessive reduction of the cross section. By applying additional kinematical cuts, the asymmetry can be enhanced to 4 %, but at the cost of a strong reduction of the cross section. Massive color-octet states can generate sizeable effects in $t\bar{t} + j$ production, both on the charge asymmetry and on the cross section. The charge asymmetry probes both vector and axial-vector couplings to quarks. We show that massive color octets can generate asymmetries up to ± 10 % for moderate and up to ± 30 % for strong kinematical cuts to be used in experimental analyses at the LHC. Jet kinematics can be used to obtain further information about the nature of the couplings and thereby to discriminate between different models.

email:
berge@uni-mainz.de
westhoff@uni-mainz.de

1 Introduction

The year 2012 was predicted to be the year of the Higgs boson. Indeed, its recent discovery at the CERN Large Hadron Collider (LHC) marks an important step towards understanding electroweak symmetry breaking – and the manifestation of the hierarchy problem. To date, it remains unclear how the electroweak scale is stabilized against large corrections from physics at higher scales. To solve this puzzle, it will be crucial to clarify whether there are new dynamics not far above the electroweak scale that trigger the Higgs mechanism. The top quark could be a messenger of such new dynamics. Due to its large mass, the top quark is suspected to take part in electroweak symmetry breaking and/or to interact strongly with new particles. Thus, probing the properties of the top quark and its couplings to the particles of the Standard Model (SM) might deliver insight into physics beyond the electroweak scale.

The experiments at the Tevatron and the LHC provide the appropriate environment for top-quark physics. With the data accumulated to date, accurate measurements of the cross section of top-quark pair production have been achieved at the center-of-mass (CM) energies of $\sqrt{s} = 1.96, 7$, and 8 TeV [1, 2]. The results are in good agreement with the equally precise SM predictions [3, 4]. Searches for new resonances in the top-antitop invariant mass spectrum both at the Tevatron and the LHC also did not reveal any hints to physics beyond the SM [5, 6, 7, 8]. The situation is less unambiguous when considering the top-quark charge asymmetry. The Tevatron collaborations CDF and DØ have measured the charge asymmetry in terms of a forward-backward asymmetry [9, 10] and found it to be larger than its SM prediction [11, 12]. Measurements of the correlated charge asymmetry at the LHC by the ATLAS and CMS collaborations do not show any deviation from the SM within the (large) experimental errors [13, 14]. Since the charge asymmetry at the LHC is very small, achieving a more precise measurement is a challenging endeavor. The Tevatron thus leaves us with a puzzle in top-quark physics that is difficult to resolve by measuring inclusive observables at the LHC.

The year 2012 will certainly also be the year of the top quark. At the LHC, top-antitop pairs are currently produced in abundance in proton-proton (pp) collisions at a CM energy of $\sqrt{s} = 8\text{ TeV}$. Due to the enlarged phase space with respect to the Tevatron, a large fraction of top-antitop pairs are produced in association with one or more hard jets. The investigation of an additional jet in $t\bar{t}$ production is interesting for very different reasons. Firstly, the process $pp \rightarrow t\bar{t} + j$ is an important background for signatures with jets, leptons and missing transverse energy, for instance in Higgs production via vector boson fusion [15] or in searches for supersymmetric particles [16]. Secondly, as the fraction of events with hard jets in inclusive $t\bar{t}$ production is sizeable, $t\bar{t} + j$ provides a good test of perturbative quantum chromodynamics at higher orders. The hadroproduction of top-quark pairs with a hard jet has been calculated in QCD to next-to-leading order (NLO) [17, 18, 19]. A first measurement of the $t\bar{t} + j$ production rate with respect to inclusive $t\bar{t}$ production by ATLAS [20] suggests that NLO corrections to $t\bar{t} + j$ production will soon be tested at the LHC. The effects of the top-quark decay and of parton showers in $t\bar{t} + j$ have been investigated in [21, 22, 23], yielding precise SM observables ready to face the experiment. Thirdly, the hard jet in $t\bar{t} + j$ production can serve to disentangle the properties of new particles that leave signatures in inclusive $t\bar{t}$ production. Following this line, CMS has recently performed a search for heavy W' bosons in

$t\bar{t} + j$ observables [24].

The purpose of this work is to investigate the charge asymmetry in $t\bar{t} + j$ production. In QCD, the charge asymmetry in $t\bar{t} + j$ arises already at leading order (LO), contrary to inclusive $t\bar{t}$ production, where the asymmetry is a NLO quantity. The forward-backward asymmetry in $t\bar{t} + j$ production at the Tevatron is sizeable because the charge-asymmetric quark-antiquark parton channel dominates the cross section. At the LHC, however, the asymmetry is strongly suppressed by the large charge-symmetric background from gluon-gluon (gg) fusion. To increase the asymmetry at the LHC, deliberate cuts on the $t\bar{t} + j$ phase space are necessary. We will perform a detailed analysis of the jet kinematics at LO and study their impact on the charge asymmetry. Based on the results, we will derive a set of suitable cuts and show that in QCD the charge asymmetry at the LHC can be increased considerably. The charge asymmetry in $t\bar{t} + j$ production in QCD is known to NLO and has been explored previously in terms of the integrated observables at the Tevatron [18, 19, 23] and the LHC [23]. The extrapolation of our results to NLO should be straightforward with the NLO amplitudes at hand.

Beyond QCD, the charge asymmetry in $t\bar{t} + j$ production can be used to discriminate between different new particles that leave signatures in top-quark pair production. We will discuss in detail the contributions of massive color-octet vector bosons with vector and axial-vector couplings to quarks. These “massive gluons” arise in various extensions of the SM in addition to the massless QCD gluons, and some may provide an explanation of the enhanced forward-backward asymmetry observed in inclusive $t\bar{t}$ production. The dominant contributions of massive gluons to the integrated charge asymmetry in $t\bar{t} + j$ production at the LHC have been discussed before in [25]. Our analysis will be based on the complete set of massive gluon contributions. We will optimize the cuts on the charge asymmetry at the LHC that project on the region where the effects of massive gluons are large. Further, we will explore the prospects of using jet kinematics in $t\bar{t} + j$ production to determine the couplings of heavy color octets.

The paper is organized as follows. Section 2 is devoted to the charge asymmetry in $t\bar{t} + j$ production in QCD. In Section 2.1, we introduce a set of phase space variables that will serve to systematically study the kinematics of $t\bar{t} + j$ production. In Section 2.2, the charge asymmetry is analyzed at parton level for the process $q\bar{q} \rightarrow t\bar{t}g$. We discuss the jet kinematics in the limit of soft and collinear gluon emission and the dependence on the gluon energy. Our findings are then applied in a numerical analysis of the charge asymmetry in $t\bar{t} + j$ production at the Tevatron (Section 2.3) and at the LHC (Section 2.4), where we suggest strategic cuts that enlarge the asymmetry. The effects of detector cuts on the charge asymmetry are analyzed in Section 2.5. Section 3 is devoted to the effects of massive color-octet bosons on the charge asymmetry in $t\bar{t} + j$ production. The generation of an asymmetry from vector and axial-vector contributions is discussed in Section 3.1. After having defined benchmark scenarios (Section 3.2), the numerical analysis of massive gluons in $t\bar{t} + j$ production is performed in Section 3.3. In Section 3.4, we show how vector and axial-vector couplings can be distinguished by jet kinematics. Finally, our conclusions are drawn in Section 4.

2 Charge asymmetry in QCD

The top-quark charge asymmetry provides a test of charge conservation or, in theories with CP symmetry, of parity conservation in top-quark pair production. The differential charge asymmetry at a fixed point in phase space is defined as the difference between the production rate of a top-antitop pair and the rate when top and antitop are interchanged. For observables at hadron colliders, the key quantity is the partonic charge-asymmetric cross section as a function of the top-/antitop-quark scattering angle θ with respect to the direction of the incident parton p_1 in the $t\bar{t}$ system,¹

$$\frac{d\hat{\sigma}_a}{d\cos\theta} = \left. \frac{d\hat{\sigma}_{t\bar{t}}}{d\cos\theta} \right|_{\theta=\theta_t^{t\bar{t}}} - \left. \frac{d\hat{\sigma}_{t\bar{t}}}{d\cos\theta} \right|_{\theta=\theta_{\bar{t}}^{t\bar{t}}}. \quad (1)$$

The charge-symmetric differential cross section $d\hat{\sigma}_s/d\cos\theta$ is defined by replacing “−” with “+” in (1). After integrating over one hemisphere,² one obtains the total normalized partonic charge asymmetry

$$\hat{A}_C(\hat{s}) = \frac{\hat{\sigma}_a(\hat{s})}{\hat{\sigma}_s(\hat{s})}, \quad \hat{\sigma}_{s/a}(\hat{s}) = \int_0^1 d\cos\theta \frac{d\hat{\sigma}_{s/a}}{d\cos\theta}, \quad (2)$$

which depends on the partonic CM energy $\sqrt{\hat{s}}$. After convoluting with the parton distribution functions (PDFs) $f_{p_i/N_i}(x_i, \mu_f)$ at the factorization scale μ_f , the hadronic charge asymmetry is given by

$$A_C = \frac{\sigma_a}{\sigma_s}, \quad \sigma_{s/a} = \sum_{p_1 p_2} \int dx_1 dx_2 f_{p_1/N_1}(x_1, \mu_f) f_{p_2/N_2}(x_2, \mu_f) \hat{\sigma}_{s/a}^{p_1 p_2}(\hat{s}, \mu_f). \quad (3)$$

The momentum fractions x_i of the partons p_i inside the nucleons N_i determine \hat{s} as a fraction of the squared CM energy of the colliding nucleons, s , via the relation $\hat{s} = x_1 x_2 s$. An asymmetry σ_a is generated in the channels $p_1 p_2 = q\bar{q}, \bar{q}q, qg, gq, \bar{q}g, g\bar{q}$; the cross section σ_s receives additional contributions from the charge-symmetric gg initial state.

Since strong interactions are charge-preserving, a charge asymmetry in QCD arises only if an additional real or virtual gluon is involved in the production process of a $t\bar{t}$ pair. In Figure 1, we show representative diagrams for contributions to the charge asymmetry from quark-antiquark ($q\bar{q}$) and quark-gluon (qg) initial parton states. The qg contribution to the charge asymmetries both at the Tevatron and at the LHC is suppressed with respect to the dominant $q\bar{q}$ channel [26, 11]. In inclusive $t\bar{t}$ production, an asymmetry is generated at NLO by both real and virtual radiative corrections (cuts marked by dotted and dashed lines), whereas in exclusive $t\bar{t} + j$ production only real radiation contributes (dotted lines). The exclusive channel $t\bar{t} + j$ thereby allows one to disentangle the (negative) real and (positive) virtual contributions to the inclusive $t\bar{t}$ asymmetry by giving separate access to the subset of real

¹The $t\bar{t}$ system is the reference frame obtained by a boost of the parton CM frame along the beam axis, where the rapidities of the top and the antitop quark are of equal magnitude, but of opposite sign.

²For $t\bar{t} + j$ production, the integration over the four remaining phase space variables is subject to a cut on the transverse momentum of the hard jet, p_T^j .

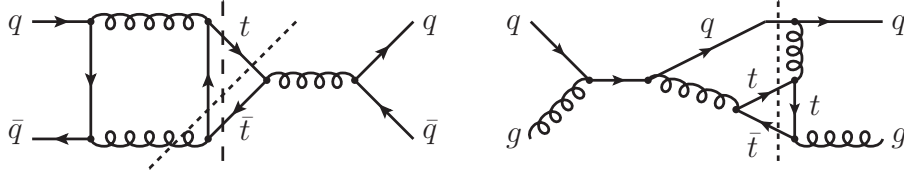


Figure 1: Charge asymmetry in hadronic top-antitop production from quark-antiquark annihilation (left) and quark excitation (right) in QCD. Shown are representative contributions to inclusive $t\bar{t}$ production (dashed and dotted cuts) and exclusive $t\bar{t} + j$ production (dotted cuts).

contributions. In the following, we will investigate the charge asymmetry in $t\bar{t} + j$ production in detail. Unless stated otherwise, we will refer to A_C defined in (3) as the exclusive asymmetry generated by real radiation only.

At hadron colliders, observables to measure the charge asymmetry have to be constructed according to the symmetry of the initial state. At the Tevatron, the charge-asymmetric proton-antiproton initial state allows one to directly access the asymmetry A_C by measuring the production rate in terms of top-antitop rapidity difference,

$$A_C^y = \frac{\sigma(\Delta y > 0) - \sigma(\Delta y < 0)}{\sigma(\Delta y > 0) + \sigma(\Delta y < 0)} = A_C, \quad \Delta y = y_t - y_{\bar{t}}. \quad (4)$$

The charge asymmetry is thus observed as a top-quark forward-backward asymmetry in the $t\bar{t}$ frame. At the LHC, one cannot probe the charge asymmetry as a forward-backward asymmetry because the proton-proton initial state is charge-symmetric. The direction of the incident quark (which sets the reference axis for the $t\bar{t}$ asymmetry) can still be determined by exploiting the quark's boost inside the proton. A top-quark “beamward-central” asymmetry can then be defined in terms of absolute rapidities³

$$A_C^{|y|} = \frac{\sigma(\Delta|y| > 0) - \sigma(\Delta|y| < 0)}{\sigma(\Delta|y| > 0) + \sigma(\Delta|y| < 0)} = \frac{\sigma_a(\Delta|y| > 0)}{\sigma_s} < A_C, \quad \Delta|y| = |y_t| - |y_{\bar{t}}|. \quad (5)$$

This observable, however, is much smaller than the Tevatron asymmetry A_C^y for two reasons: Firstly, $A_C^{|y|}$ is defined in the laboratory (lab) frame and is therefore diluted by the boost with respect to the $t\bar{t}$ frame, resulting in $A_C^{|y|} < A_C$. Secondly and mainly, the charge-symmetric gg background at the LHC is much larger than at the Tevatron, yielding $A_C^{(\text{LHC})} \ll A_C^{(\text{Tevatron})}$.

2.1 Phase space variables and cuts

The strong suppression of the total charge asymmetry at the LHC can be relaxed by applying suitable cuts on the final-state phase space. In particular, the jet kinematics can be used to enhance the asymmetry in $t\bar{t} + j$ production. In this section, we define a set of cuts in terms

³The notation $\sigma_a(\Delta|y| > 0)$ is to be understood as $\sigma_a(\Delta|y| > 0) = \sigma_{t\bar{t}(j)}(|y_t| > |y_{\bar{t}}|) - \sigma_{t\bar{t}(j)}(|y_{\bar{t}}| > |y_t|)$.

of phase space variables that allows one to systematically probe the kinematic behavior of the cross section σ_s and the charge asymmetries A_C^y and $A_C^{|y|}$ at the Tevatron and the LHC.

The phase space of the partonic process $p_1 p_2 \rightarrow t\bar{t}j$ can be expressed in terms of five variables in the $p_1 p_2$ CM frame. We choose these variables to be the jet and top-quark energies, E_j and E_t , the jet and top-quark scattering angles with respect to the incident parton p_1 , θ_j and θ_t , and the azimuthal angle of the top quark, ϕ_t . Hadronic observables depend on two further variables: the boost of the partonic CM frame with respect to the lab frame, $\beta = (x_1 - x_2)/(x_1 + x_2)$, and the squared CM energy of the $p_1 p_2$ pair, \hat{s} . Both these variables are fixed by the momentum fractions x_1 and x_2 carried by the partons inside the colliding hadrons.

The top-quark energy E_t and the scattering angle θ_t , as well as their counterparts $E_{\bar{t}}$ and $\theta_{\bar{t}}$ for the antitop quark, determine the rapidities in the $p_1 p_2$ CM frame,

$$\hat{y}_t = \frac{1}{2} \ln \left(\frac{1 + \sqrt{1 - m_t^2/E_t^2} \cos \theta_t}{1 - \sqrt{1 - m_t^2/E_t^2} \cos \theta_t} \right) \quad \text{and} \quad \hat{y}_{\bar{t}} = \frac{1}{2} \ln \left(\frac{1 + \sqrt{1 - m_t^2/E_{\bar{t}}^2} \cos \theta_{\bar{t}}}{1 - \sqrt{1 - m_t^2/E_{\bar{t}}^2} \cos \theta_{\bar{t}}} \right). \quad (6)$$

The rapidities that define the charge asymmetries in (4) and (5) are obtained after boosting \hat{y}_t and $\hat{y}_{\bar{t}}$ to the lab frame via $y_{t/\bar{t}} = \hat{y}_{t/\bar{t}} + y_{t\bar{t}j}$, with $y_{t\bar{t}j}$ defined in Appendix A. As the charge asymmetry increases with the rapidity difference Δy ($\Delta|y|$), a lower cut on this quantity helps to enhance A_C^y ($A_C^{|y|}$). This cut does not involve the jet kinematics and is thus equally applicable in inclusive $t\bar{t}$ and exclusive $t\bar{t} + j$ production.

Jet kinematics are parameterized by the jet energy E_j and the scattering angle θ_j . The production cross section σ_s is particularly sensitive to both variables, due to the logarithmic enhancement in the region where $E_j \rightarrow 0$ and/or $\theta_j \rightarrow 0$. We postpone a detailed discussion of this behavior to Section 2.2 and limit ourselves here to expressing E_j and θ_j in terms of lab-frame quantities that are suitable for experimental cuts. At LO, the jet energy E_j is related to the (frame-independent) invariant mass $M_{t\bar{t}}$ of the top-antitop pair via

$$M_{t\bar{t}}^2 = (p_t + p_{\bar{t}})^2 \stackrel{\text{LO}}{=} \hat{s} (1 - 2E_j/\sqrt{\hat{s}}), \quad (7)$$

where p_t and $p_{\bar{t}}$ denote the four-momenta of the top and antitop quarks. A lower cut on $M_{t\bar{t}}$ implies an upper bound on the jet energy E_j . The dependence of the asymmetry on $M_{t\bar{t}}$ is mild in QCD, but becomes important in the search for massive resonances. We will elaborate on this point in Section 3.

The jet scattering angle θ_j encodes important information about the asymmetry in the collinear limit $\theta_j \rightarrow 0$. The jet rapidity in the partonic CM frame, \hat{y}_j , is directly related to the angle θ_j . For experimental purposes, it is convenient to express rapidities in the parton frame in terms of rapidity differences that can be measured in the lab frame, the latter being invariant under boosts along the beam axis. Here we exploit the feature that the rapidity of the system of final-state particles in the parton frame vanishes, which at LO implies $\hat{y}_{t\bar{t}j} = 0$.⁴ The parton-frame rapidity \hat{y}_j can then be described conveniently in terms of the lab-frame

⁴The definition of $\hat{y}_{t\bar{t}j}$ is given as for $y_{t\bar{t}j}$ in Appendix A by interpreting the momenta as given in the parton frame.

rapidities y_j and $y_{t\bar{t}j}$ as

$$\hat{y}_j = \frac{1}{2} \ln \left(\frac{1 + \cos \theta_j}{1 - \cos \theta_j} \right) \stackrel{\text{LO}}{=} \hat{y}_j - \hat{y}_{t\bar{t}j} = y_j - y_{t\bar{t}j}. \quad (8)$$

As we will show in Section 2.2, the QCD charge asymmetry is maximal if the jet is emitted perpendicular to the beam axis. A cut on the jet rapidity \hat{y}_j is therefore suitable to enhance the integrated charge asymmetry in QCD.

The azimuthal angle of the top quark ϕ_t is not observable at hadron colliders because the experimental setup is symmetric under rotations around the beam axis. What can be observed is the azimuthal correlation between the particles in the final state, for instance the difference between the azimuthal angles of the top quark and the antitop quark, $\Delta\phi_{t\bar{t}} = \phi_t - \phi_{\bar{t}}$. For fixed transverse momenta $p_T^t = E_t \sin \theta_t$ and $p_T^{\bar{t}} = E_{\bar{t}} \sin \theta_{\bar{t}}$, this azimuthal difference can be expressed in terms of the jet transverse momentum $p_T^j = E_j \sin \theta_j$ via

$$(p_T^j)^2 \stackrel{\text{LO}}{=} (p_T^{t\bar{t}})^2 = (p_T^t)^2 + (p_T^{\bar{t}})^2 + 2 p_T^t p_T^{\bar{t}} \cos \Delta\phi_{t\bar{t}}. \quad (9)$$

The dependence of the charge asymmetry on p_T^j will be discussed in Section 2.5. Azimuthal correlation in terms of $\Delta\phi_{t\bar{t}}$ will not be a subject of this work.

The boost β of the partonic CM frame with respect to the lab frame helps to discriminate between different partonic initial states [27]. It is related to the lab-frame rapidity of the $t\bar{t} + j$ system, $y_{t\bar{t}j}$, via

$$y_{t\bar{t}j} \stackrel{\text{LO}}{=} \frac{1}{2} \ln \left(\frac{1 + \beta}{1 - \beta} \right), \quad \text{with} \quad \beta = \frac{x_1 - x_2}{x_1 + x_2}. \quad (10)$$

The derivation, as well as an illustration of the relation between β and $y_{t\bar{t}j}$ are given in Appendix A. Accordingly, a lower cut on $|y_{t\bar{t}j}|$ selects events with a strong boost β along the beam line. It increases the weight of the partonic states with a boosted valence quark, i.e. $q\bar{q}$ and qg , and thereby enhances the charge asymmetry over its gg background. This feature is thus of particular importance at the LHC, where the fraction of gg initial states dominates the $t\bar{t} + j$ production cross section.

Besides the above-mentioned “strategic” cuts, the design of the detector and the methods of jet reconstruction require additional cuts on the jet properties. If not stated otherwise, we work with the following cuts on the jet rapidity y_j and the transverse momentum p_T^j . For Tevatron observables, we employ $|y_j| \leq 2$ and $p_T^j \geq 20 \text{ GeV}$, for the LHC we use $|y_j| \leq 2.5$ and $p_T^j \geq 25 \text{ GeV}$. The rapidity cut prevents the jet from being emitted parallel to the beam axis, enforcing $\theta_j \neq 0$, whereas the transverse momentum cut imposes a minimum jet energy $E_j > 0$ for a given jet direction. For our numerical analysis, we set the factorization and renormalization scales equal to the top-quark mass $\mu_f = \mu_r = m_t = 173.2 \text{ GeV}$ [28]. Since all calculations are done at LO, we use CTEQ6L1 PDFs [29] with an input of the strong coupling constant $\alpha_s(m_t) = 0.1180$. The phase-space integration is performed numerically by means of the Vegas Monte-Carlo algorithm implemented in [30, 31].

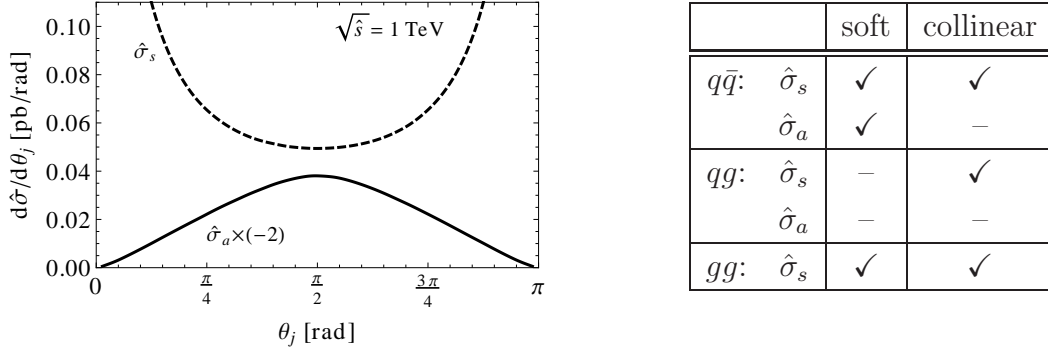


Figure 2: Left: Jet angular distribution in QCD for the partonic process $q\bar{q} \rightarrow t\bar{t}g$ as a function of the scattering angle θ_j for $\sqrt{s} = 1$ TeV and $p_T^j \geq 2$ GeV. The charge-asymmetric cross section $\hat{\sigma}_a$ (solid line) is rescaled by a factor of -2 . Right: Soft and collinear singularities of the charge-symmetric ($\hat{\sigma}_s$) and -asymmetric ($\hat{\sigma}_a$) contributions to $t\bar{t} + j$ production from $q\bar{q}$, qg , and gg initial states.

2.2 Anatomy of $t\bar{t} + j$ production at parton level: the jet handle

Before turning to measurable quantities, we discuss in detail the kinematics of the emitted gluon in the partonic process $q\bar{q} \rightarrow t\bar{t}g$, which yields the dominant contribution to the top-quark charge asymmetry. At the parton level, the features of the cross section and the asymmetry are not diluted by boosts along the beam axis or by the ignorance of the quark direction. Due to the occurrence of singularities in the infrared limit, a good understanding of the kinematics is crucial in the region where the emitted gluon is soft, $E_j \rightarrow 0$, or (anti-)collinear to the incident quark, $\theta_j \rightarrow \{0, \pi\}$. The infrared behavior of the charge-symmetric and -asymmetric cross section for different partonic initial states is summarized in the table in Figure 2. In the $q\bar{q}$ and gg channels, the charge-symmetric cross section $\hat{\sigma}_s$ exhibits both soft and collinear singularities. The charge-asymmetric cross section $\hat{\sigma}_a$, arising from the diagrams shown in Figure 1, is finite in the collinear limit $\theta_j \rightarrow \{0, \pi\}$. The differing collinear behavior of $\hat{\sigma}_s$ and $\hat{\sigma}_a$ is reflected by the angular distribution of the gluon,

$$\frac{d\hat{\sigma}_{s/a}}{d\theta_j} = \frac{d\hat{\sigma}_{s/a}(\cos\theta_t^{t\bar{t}} > 0)}{d\theta_j} \pm \frac{d\hat{\sigma}_{s/a}(\cos\theta_t^{t\bar{t}} < 0)}{d\theta_j}, \quad (11)$$

which is displayed in Figure 2 for the partonic process $q\bar{q} \rightarrow t\bar{t}g$. The symmetric cross section $\hat{\sigma}_s$ (dashed line) is enhanced if the gluon is emitted along the beam line, which is due to the collinear singularity in the limit $\theta_j \rightarrow \{0, \pi\}$. The asymmetric cross section $\hat{\sigma}_a$ (solid line) does not exhibit this collinear enhancement and reaches its maximum if the gluon is emitted perpendicular to the beam line. Since QCD is invariant under CP conjugation, the angular distribution of the emitted parton from the (CP-symmetric) $q\bar{q}$ and gg initial states is symmetric under $\theta_j \leftrightarrow \pi - \theta_j$ for both $\hat{\sigma}_s$ and $\hat{\sigma}_a$.

A cut on the transverse momentum of the jet, $p_T^j = E_j \sin\theta_j$, simultaneously regularizes soft and collinear divergences. In the region of a low transverse momentum, QCD predicts a

double-logarithmic enhancement of the charge-symmetric total cross section σ_s and a single-logarithmic enhancement of the asymmetric cross section σ_a [19],

$$\sigma_s(p_T^j) \sim \ln\left(\frac{m_t}{p_T^j}\right)_{\text{soft}} \cdot \ln\left(\frac{m_t}{p_T^j}\right)_{\text{coll.}}, \quad \sigma_a(p_T^j) \sim \ln\left(\frac{m_t}{p_T^j}\right)_{\text{soft}}. \quad (12)$$

The interplay of collinear and soft divergences is shown in Figure 3 for the parton channel $q\bar{q} \rightarrow t\bar{t}g$. In this channel, the partonic cross sections $\hat{\sigma}_s$ and $\hat{\sigma}_a$ feature the same infrared behavior as the hadronic quantities σ_s and σ_a in (12). We display the partonic charge asymmetry \hat{A}_C defined in (2) (left panel) and the cross section $\hat{\sigma}_s$ (right panel) as a function of the gluon scattering angle θ_j and the gluon energy E_j , the latter being connected to the invariant mass $M_{t\bar{t}}$ via (7). The double-logarithmic enhancement of $\hat{\sigma}_s$ from (12) is visible in the regions where $E_j \rightarrow 0$ and $\theta_j \rightarrow \{0, \pi\}$. The charge asymmetry \hat{A}_C shows a mild dependence on E_j or $M_{t\bar{t}}$, unless E_j ($M_{t\bar{t}}$) is very large (small). In the soft-gluon limit, where most of the CM energy \sqrt{s} is carried by the $t\bar{t}$ pair, the logarithmic enhancement of $\hat{\sigma}_s$ and $\hat{\sigma}_a$ from (12) cancels in the ratio \hat{A}_C . The normalized asymmetry is thus largely unaffected by a variation of the gluon energy E_j in the soft region. The low sensitivity to E_j or $M_{t\bar{t}}$ translates to the hadronic asymmetries A_C^y and $A_C^{|y|}$, as the $t\bar{t} + j$ cross section σ_s is dominated by soft jets (cf. Figure 3, right). Still, a lower cut on $M_{t\bar{t}}$ increases the asymmetry, as it projects on the region of soft-gluon emission even for larger CM energies, which yields the dominant contribution. The dependence of the charge asymmetry on θ_j , in turn, is strong. Due to the collinear enhancement of $\hat{\sigma}_s$, but not of $\hat{\sigma}_a$, the charge asymmetry $\hat{A}_C \sim \ln^{-1}(m_t/p_T^j)$ vanishes in the limit $\theta_j \rightarrow \{0, \pi\}$. The maximum of \hat{A}_C is reached for $\theta_j = \pi/2$ due to the synergy of two effects: Firstly, $\hat{\sigma}_a$ is maximal for a gluon emitted perpendicular to the beam axis and secondly, $\hat{\sigma}_s$ entering the normalization is depleted in the central region (cf. Figure 2, left). A lower cut on the gluon scattering angle θ_j , or equivalently on the jet rapidity \hat{y}_j from (8) for hadronic observables, therefore increases the charge asymmetry. In addition, it has the beneficial feature of focusing on the collinear-safe region, where the asymmetry is not affected by logarithmic divergences. In the collinear limit $\theta_j \rightarrow \{0, \pi\}$, in turn, large logarithms should be resummed in order to make a reliable prediction of the charge asymmetry in this region.

2.3 Forward-backward asymmetry at the Tevatron

Top-quark pair production at the Tevatron proceeds mainly through the partonic channel $q\bar{q}$. This feature is due to the CM energy of $\sqrt{s} = 1.96$ TeV, where the gg channel is suppressed by the PDFs, and to the fact that both q and \bar{q} are valence quarks in the initial hadronic state $p\bar{p}$. The total cross section for the process $p\bar{p} \rightarrow t\bar{t} + j$ in QCD at LO is $\sigma_s^{\text{LO}} = 1.63_{-0.54}^{+0.99}$ pb for $p_T^j \geq 20$ GeV,⁵ where the respective contributions of the partonic channels amount to 83% ($q\bar{q}$), 10% ($qg + \bar{q}g$), and 7% (gg). At NLO, the cross section is given by $\sigma_s^{\text{NLO}} = 1.791(1)_{-0.31}^{+0.16}$ pb [18],⁶ which constitutes about 26 % of the total cross section for inclusive $t\bar{t}$ production [4].

⁵The uncertainties on σ_s^{LO} and $A_C^{y,\text{LO}}$ (as well as on σ_s^{LO} and $A_C^{|y|,\text{LO}}$ in Section 2.4) are due to the scale variations $m_t/2 < \mu_f = \mu_r < 2m_t$. No detector cut on $|y_j|$ has been applied in order to allow a comparison with the NLO results from [18] and [23].

⁶The results for σ_s^{NLO} and $A_C^{y,\text{NLO}}$ are obtained with $m_t = 174$ GeV and CTEQ6M PDFs.

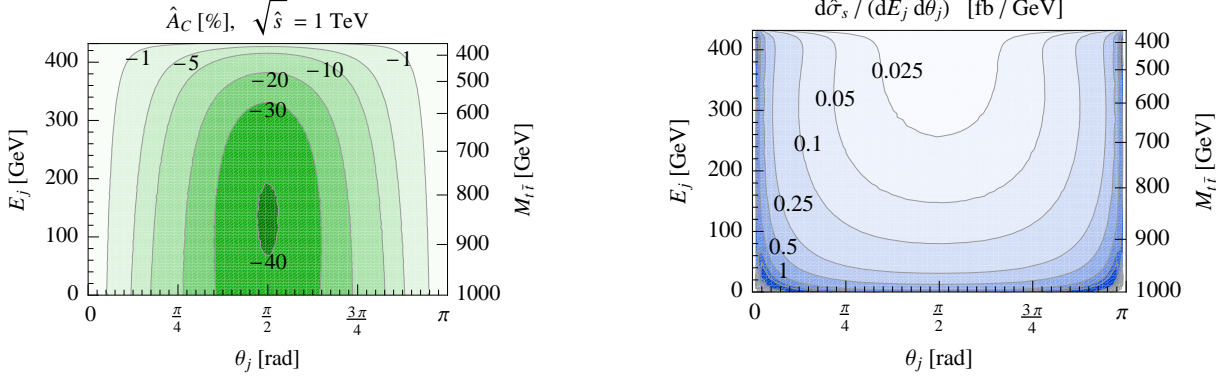


Figure 3: The partonic process $q\bar{q} \rightarrow t\bar{t}g$ for $\sqrt{s} = 1$ TeV and $p_T^j \geq 2$ GeV as a function of the gluon scattering angle θ_j , the gluon energy E_j , and the invariant mass $M_{t\bar{t}}$. Left: Partonic charge asymmetry \hat{A}_C [%]. Right: Charge-symmetric cross section $d\hat{\sigma}_s / (dE_j d\theta_j)$ [fb/GeV].

The QCD prediction of the total cross section agrees with the measurement by the CDF collaboration, $\sigma_s = 1.6 \pm 0.2 \pm 0.5$ pb [32]. The integrated charge asymmetry defined in (4) amounts to $A_C^{y,\text{LO}} = -11.1_{-0.1}^{+0.2}$ % at LO. It is affected by large NLO QCD corrections, yielding $A_C^{y,\text{NLO}} = -4.40 \pm 0.04$ % [23]. This large reduction is of the order of the charge asymmetry in inclusive $t\bar{t}$ production, $A_C^{y,t\bar{t}} \approx 7$ %. It does not signal a breakdown of the perturbative framework, but is due to contributions from virtual hard-gluon corrections [19].

In the following, we discuss the dependence of the Tevatron asymmetry on the jet kinematics. The low gg background and the equivalence of the charge asymmetry A_C and the forward-backward asymmetry A_C^y from (4) allow us to apply our findings for the partonic channel $q\bar{q} \rightarrow t\bar{t}g$ from Section 2.2 directly to the hadronic observables. We saw that the asymmetry is strongly dependent on the jet rapidity. In the left panel in Figure 4, we show the charge asymmetry A_C^y as a function of the jet rapidity in the partonic CM frame \hat{y}_j (solid black curve), compared to the lab-frame rapidity y_j (dashed black curve). The difference between \hat{y}_j and y_j is given by the boost of the parton frame encoded in the rapidity $y_{t\bar{t}j}$, as has been shown in (8). Due to this boost, the distribution in terms of the lab-frame rapidity y_j is washed out with respect to the parton-frame rapidity \hat{y}_j . The latter distribution reaches its maximum if the jet is emitted perpendicular to the beam axis, yielding $A_C^y(\hat{y}_j = 0) = -27$ %. An upper cut on $|\hat{y}_j|$ is therefore well suited to enhance the asymmetry, though at the cost of reducing the cross section σ_s displayed on the right-hand side in Figure 4. Notice that due to the significant dependence on y_j , the integrated charge asymmetry is very sensitive to the detector cut $|y_j| \leq 2$.

As discussed in Section 2.2, the asymmetry can also be enhanced by performing cuts on the invariant mass $M_{t\bar{t}}$, related to the jet energy E_j via (7), and on the top-antitop rapidity difference Δy . In Table 1, we display the Tevatron charge asymmetry A_C^y and the cross section σ_s for cuts on $|\hat{y}_j|$, $M_{t\bar{t}}$ and $|\Delta y|$. This sample allows us to compare the various cuts with respect to their efficiency to enhance the charge asymmetry, while keeping the reduction of the cross section moderate. The second, fourth and fifth columns of the table show that a cut

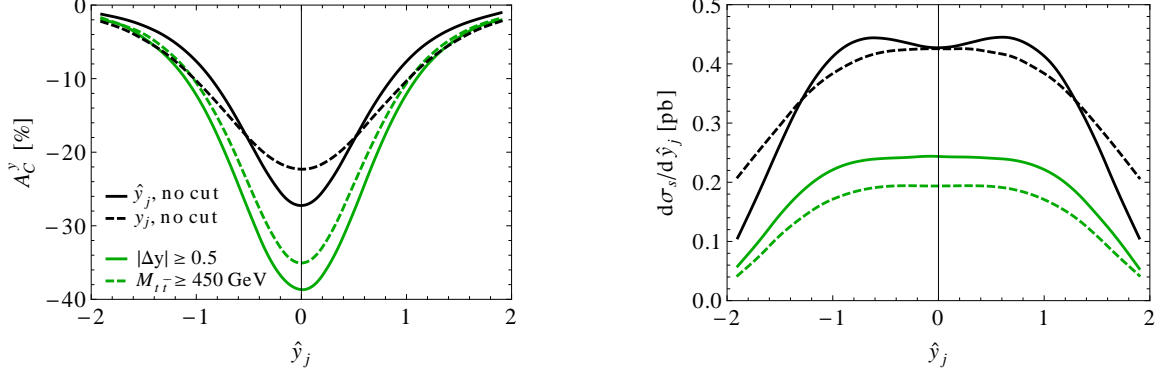


Figure 4: Charge asymmetry A_C^y (left) and differential cross section $d\sigma_s/d\hat{y}_j$ (right) for $t\bar{t} + j$ production at the Tevatron as a function of the jet rapidity in the parton CM frame \hat{y}_j (black) and the lab frame y_j (dashed black). Additional cuts on the $t\bar{t}$ rapidity difference Δy (invariant mass $M_{t\bar{t}}$) are shown for the \hat{y}_j distributions in green (dashed green). Detector cuts of $|y_j| \leq 2$ and $p_T^j \geq 20$ GeV have been applied for all distributions.

on $|\hat{y}_j|$ can enhance A_C^y from -12.6% to the -20% level, but simultaneously reduces σ_s by about a factor of two or more. Comparing with the third column, one observes that a cut on $M_{t\bar{t}}$ is less efficient than $|\hat{y}_j|$ in enhancing the charge asymmetry for a given cross section. The efficiency of cuts on $|\hat{y}_j|$ and $|\Delta y|$ (columns four and six) is almost the same for cross sections down to $\sigma_s = 0.4$ pb, or equivalently for $|\hat{y}_j|^{\max} \geq 0.5$ and $|\Delta y|^{\min} \leq 0.8$. By comparing the fifth and the last columns, it is apparent that a combination of cuts on $|\hat{y}_j|$ and $|\Delta y|$ is more efficient to enhance the asymmetry for a fixed cross section than a stronger cut on $|\hat{y}_j|$ alone. The effect of additional cuts on $M_{t\bar{t}}$ and $|\Delta y|$ is illustrated in Figure 4, where $A_C^y(\hat{y}_j)$ and $d\sigma_s/d\hat{y}_j$ are displayed for $|\Delta y| \geq 0.5$ (green curves) and $M_{t\bar{t}} \geq 450$ GeV (dashed green curves). Due to the low $t\bar{t} + j$ production rate at the Tevatron, however, a measurement of the charge asymmetry and its kinematical features remains an experimental challenge.

The charge asymmetry in $t\bar{t} + j$ production has been investigated before in [23] at NLO QCD including parton showering. The enhancement of A_C^y for the applied cuts $M_{t\bar{t}} \geq 450$ GeV and $|\Delta y| \geq 1.0$ qualitatively agrees with our findings at LO. Numerically, however, the NLO results for A_C^y differ significantly from our LO results due to the large shift of the asymmetry by NLO corrections. In order to obtain precise QCD predictions of the charge asymmetry for

	no cuts	$M_{t\bar{t}} \geq 450$ GeV	$ \hat{y}_j \leq 1$	$ \hat{y}_j \leq 0.5$	$ \Delta y \geq 0.5$	$ \hat{y}_j \leq 1, \Delta y \geq 0.5$
A_C^y [%]	-12.6	-17.0	-18.2	-24.0	-19.1	-27.5
σ_s [pb]	1.42	0.61	0.87	0.43	0.78	0.48

Table 1: Charge asymmetry A_C^y and cross section σ_s at the Tevatron for cuts on the invariant mass $M_{t\bar{t}}$, the partonic jet rapidity \hat{y}_j , and the rapidity difference $\Delta y = y_t - y_{\bar{t}}$.

the cuts suggested in this work, an analysis of the kinematic distributions at NLO would be necessary.

2.4 Beamward-central asymmetry at the LHC

The difficulty in observing a hard jet in $t\bar{t}$ production at the Tevatron is overcome at the LHC by a much larger production rate. The QCD observables for the process $pp \rightarrow t\bar{t} + j$ have been previously calculated at NLO for a CM energy of $\sqrt{s} = 7$ TeV and a cut on the jet transverse momentum $p_T^j \geq 50$ GeV. At LO, the total cross section is given by $\sigma_s^{\text{LO}} = 40.9_{-13.2}^{+23.6}$ pb. This is to be compared with the cross section at NLO, $\sigma_s^{\text{NLO}} = 53.1(2)_{-8.9}^{+4.1}$ pb [23],⁷ which makes up 29 % of the inclusive $t\bar{t}$ cross section at NLO given in [4]. The fraction of $t\bar{t} + j$ events in the inclusive $t\bar{t}$ sample increases when lowering the cut on p_T^j . Compared to $t\bar{t}$ production at the Tevatron, the contribution of $t\bar{t} + j$ is larger due to the enlarged phase space for the production of a hard jet at higher collision energies. The charge asymmetry defined in (5) is given at LO by $A_C^{|y|, \text{LO}} = -0.47 \pm 0.04$ %. The large contribution of virtual gluon corrections at NLO causes a sign shift, yielding $A_C^{|y|, \text{NLO}} = 0.51 \pm 0.09$ % [23].

We will perform our analysis of the charge asymmetry at the LHC for $\sqrt{s} = 8$ TeV (LHC8), $p_T^j \geq 25$ GeV, and a detector cut of $|y_j| \leq 2.5$. The total cross section at LO is given by $\sigma_s^{\text{LO}} = 97.5_{-30.6}^{+54.0}$ pb. Compared to the result for $\sqrt{s} = 7$ TeV and $p_T^j \geq 50$ GeV, the cross section is enhanced by the increased CM energy, but mainly due to the relaxed cut on the transverse momentum of the jet. The respective partonic channels contribute to the cross section with 7.7% ($q\bar{q}$), 26.7% ($qg + \bar{q}g$) and 65.6% (gg). The charge asymmetry is given by $A_C^{|y|, \text{LO}} = -0.56 \pm 0.5$ %. As was explained previously, the strong suppression of the charge asymmetry at the LHC is mainly due to the large charge-symmetric gg background and to the fact that the asymmetry in the qg channel is tiny. Thus, in order to observe a sizeable charge asymmetry in $t\bar{t} + j$ production at the LHC, the application of cuts is indispensable.

Similarly to what we observed for the Tevatron, the observables at the LHC are strongly dependent on the jet kinematics. In particular, the jet rapidity distribution of the charge asymmetry and the cross section is determined by the collinear behavior. In Figure 5, we show $A_C^{|y|}$ (left) and σ_s (right) as a function of the jet rapidity in the parton frame, \hat{y}_j , for the detector cuts $|y_j| \leq 2.5$ and $p_T^j \geq 25$ GeV. Without further cuts (black curve), the charge asymmetry reaches its maximum for a central jet, $A_C^{|y|}(\hat{y}_j = 0) = -1.5$ %. With respect to the total asymmetry $A_C^{|y|} = -0.56$ %, the asymmetry is enhanced by almost a factor of three, but remains a small quantity due to the high gg suppression. As was explained in Section 2.1, the charge-symmetric background can be reduced by filtering out highly-boosted $q\bar{q}$ events through a lower cut on the boost rapidity $y_{t\bar{t}j}$ defined in Appendix A. For instance, by restricting the rapidity to $|y_{t\bar{t}j}| \geq 0.5$ (dashed red curve), the maximal charge asymmetry increases to $A_C^{|y|}(\hat{y}_j = 0, |y_{t\bar{t}j}| \geq 0.5) = -2.3$ %. The cross section is simultaneously reduced by a factor of two.

In addition or alternatively to selecting boosted $q\bar{q}$ parton contributions, the asymmetry can be enhanced by exploiting the kinematics of the $t\bar{t} + j$ final state. In the left panel of Figure 6, we compare the efficiency of cuts on different variables v to generate a large charge

⁷The result for σ_s^{NLO} includes effects from parton showering.

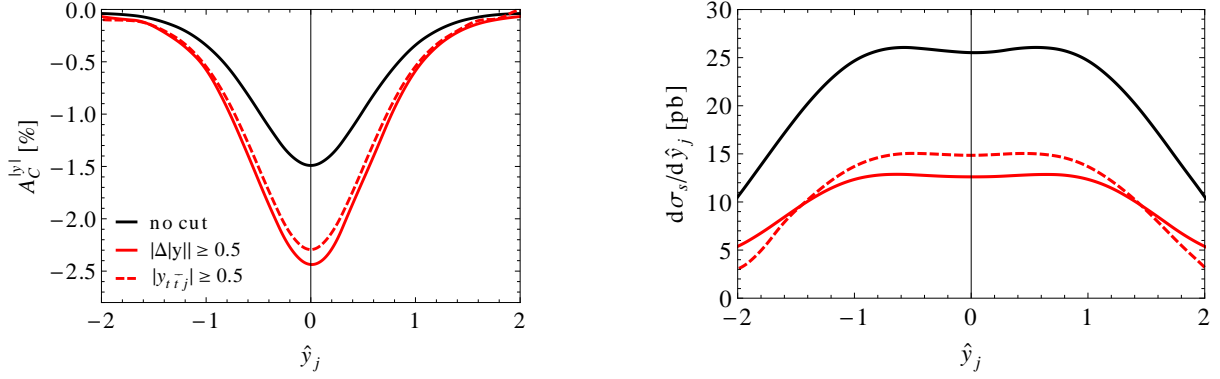


Figure 5: Charge asymmetry $A_C^{[y]}$ (left) and cross section σ_s (right) for $t\bar{t} + j$ production at LHC8 as a function of the parton-frame rapidity \hat{y}_j without (black) and with additional cuts on the parton-frame boost $|y_{t\bar{t}j}|$ (red) and the difference between absolute t and \bar{t} rapidities $|\Delta|y|$ (dashed red). Detector cuts of $|y_j| \leq 2.5$ and $p_T^j \geq 25$ GeV have been applied for all distributions.

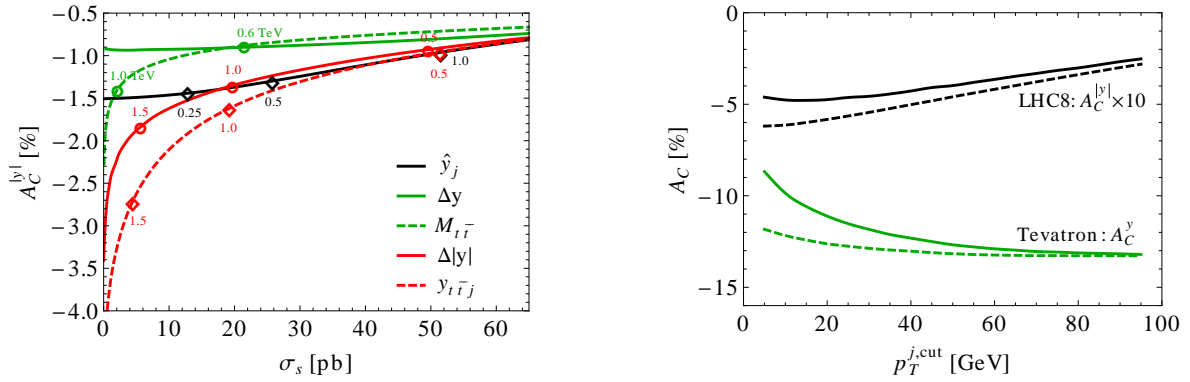


Figure 6: Left: Integrated charge asymmetry $A_C^{[y]}$ at the LHC8 as a function of the cross section σ_s for cuts on kinematic variables v . Numbers mark the cuts v^{\min} , v^{\max} , i.e. $|v| \geq v^{\min}$ ($|v| \leq v^{\max}$ for $v = \hat{y}_j$). Right: Charge asymmetry as a function of the minimal jet transverse momentum, $p_T^{j,\text{cut}}$, at the Tevatron (green) and the LHC8 (black, rescaled by a factor of 10), without further cuts (solid) and with the jet rapidity cuts $|y_j| \leq 2$ (dashed green) and $|y_j| \leq 2.5$ (dashed black).

asymmetry $A_C^{[y]}$ for a given cross section σ_s . We compare cuts on the jet rapidity \hat{y}_j , the top-antitop rapidity difference Δy and invariant mass $M_{t\bar{t}}$, which were already relevant for the Tevatron asymmetry. In addition, we introduce cuts on the difference between absolute top and antitop rapidities $\Delta|y|$ and the parton-frame boost rapidity $y_{t\bar{t}j}$, which are adapted to the experimental setup at the LHC. The numbers in the figure indicate the cuts v^{\min} , v^{\max} corresponding to the point $\{\sigma_s, A_C^{[y]}\}(|v| \geq v^{\min})$ for $v = \Delta y, M_{t\bar{t}}, \Delta|y|, y_{t\bar{t}j}$ and $\{\sigma_s, A_C^{[y]}\}(|v| \leq v^{\max})$ for $v = \hat{y}_j$. As for the Tevatron, the charge asymmetry $A_C^{[y]}$ is not very sensitive to a cut on the invariant mass $M_{t\bar{t}}$ (dashed green curve), unless one enters the regime where the

	no cuts	$ \hat{y}_j \leq 0.5$	$ \Delta y \geq 1$	$ y_{t\bar{t}j} \geq 1$		
				–	$ \hat{y}_j \leq 0.5$	$ \hat{y}_j \leq 0.5 \leq \Delta y $
$A_C^{[y]} [\%]$	–0.56	–1.30	–1.35	–1.62	–2.91	–4.04
$\sigma_s [\text{pb}]$	97.5	25.7	19.7	19.2	6.63	4.00

Table 2: Charge asymmetry $A_C^{[y]}$ and cross section σ_s at LHC8 for cuts on the partonic jet rapidity \hat{y}_j , the rapidity difference $\Delta|y| = |y_t| - |y_{\bar{t}}|$, and the boost of the parton frame $y_{t\bar{t}j}$. Detector cuts of $|y_j| \leq 2.5$ and $p_T^j \geq 25 \text{ GeV}$ have been applied.

emitted jet is soft (cf. Figure 3). For such a strong cut on $M_{t\bar{t}}$, however, the cross section is very small. A lower cut on Δy (solid green curve), the variable defining the forward-backward asymmetry at the Tevatron, selects $t\bar{t}$ pairs that are emitted back-to-back and parallel to the beam axis. At the LHC, this cut is not efficient, because the definition of the charge asymmetry in terms of $\Delta|y|$ involves top and antitop quarks that are scattered perpendicular to the beam axis. It is thus more suitable to focus on events where one of the top and antitop quarks is beam-like, while the other quark is central, i.e. on events with a large difference of absolute rapidities $\Delta|y|$. For cross sections $\sigma_s \geq 20 \text{ pb}$ (corresponding to $\Delta|y|^{\min} \leq 1.0$), a lower cut on $\Delta|y|$ (solid red curve) is almost as efficient in increasing $A_C^{[y]}$ as the jet rapidity \hat{y}_j (black curve). For the regime close to the kinematic endpoint, where the cross section is very small, the cut on $\Delta|y|$ is more efficient. The most efficient variable is the boost rapidity $y_{t\bar{t}j}$ (dashed red curve). For cross sections $\sigma_s \geq 30 \text{ pb}$, cuts on $y_{t\bar{t}j}$ and \hat{y}_j are of comparable efficiency. With a very strong cut $y_{t\bar{t}j} \gtrsim 2$, a maximal asymmetry of $A_C^{[y]} \approx -4\%$ can be achieved. As for the Tevatron, the combination of cuts on several variables is more efficient to increase the asymmetry than a stronger cut on one single variable. Combinations of the most efficient variables $y_{t\bar{t}j}$ and $\Delta|y|$ with \hat{y}_j are given in Figure 5 (solid and dashed red curves). In Table 2, we display $A_C^{[y]}$ and σ_s for various cuts corresponding to the points indicated in Figure 6, left. To demonstrate the power of combinations of cuts, in the last two columns we give the results for $|y_{t\bar{t}j}| \geq 1$ with the simultaneous cuts $|\hat{y}_j| \leq 0.5$ and $|\hat{y}_j| \leq 0.5, |\Delta|y|| \geq 0.5$. For similar cross sections, the resulting charge asymmetries of $A_C^{[y]} = -2.91\%$ and -4.04% cannot be achieved by a single cut on either of the variables $|y_{t\bar{t}j}|$, $|\hat{y}_j|$ or $|\Delta|y||$, as can be read off from Figure 6, left. Generically, the charge asymmetry hardly exceeds -5% , even for very strong cuts on the cross section. Since NLO corrections cause a positive shift, the absolute value of a cut charge asymmetry beyond LO is expected to be rather smaller. A measurement of the QCD charge asymmetry in $t\bar{t} + j$ production at the LHC will therefore be difficult. Yet, as we will see in Section 3, the smallness of the QCD charge asymmetry can be turned into a virtue in the search for new particles that can generate large effects on $A_C^{[y]}$.

2.5 Experimental cuts on jet properties

We conclude our analysis of the QCD charge asymmetry by discussing its dependence on cuts on the jet properties conditioned by the experimental setup. A cut on the jet rapidity $|y_j|$ takes account of the tracking capacity of the inner detector in the forward region, which is limited to $|y_j| \leq 2$ at CDF ($|y_j| \leq 2.5$ at DØ) and to $|y_j| \leq 2.5$ at ATLAS ($|y_j| \leq 2.4$ at CMS). For the Tevatron, the effect of varying the cut on $|y_j|$ can be estimated by looking at the dashed black curve in Figure 4. A stronger cut discards the region where σ_a is small and thereby yields a larger asymmetry A_C^y . Analogous considerations apply for variations of the jet rapidity cut at the LHC.

A further cut is required on the transverse momentum of the jet, $p_T^j = E_j \sin \theta_j$, in order to avoid misidentification due to the pile-up background in the forward region. The cuts used by the experimental collaborations for top-quark pair production are given by $p_T^j \geq 20$ GeV (CDF and DØ), $p_T^j \geq 25$ GeV (ATLAS) and $p_T^j \geq 30$ GeV (CMS). The dependence of the top-quark charge asymmetry on p_T^j can be understood by analyzing its asymptotic behavior at low and high jet transverse momenta. At low p_T^j , the charge asymmetry is dominated by the collinear limit $\theta_j \rightarrow 0$ described in (12), yielding $A_C \sim \ln^{-1}(m_t/p_T^j)$. The charge asymmetry therefore increases with increasing p_T^j . High transverse momenta p_T^j correspond to high jet energies E_j where the asymmetry is suppressed (see Figure 3, left). In this regime, the charge asymmetry thus decreases with increasing p_T^j .

In the right panel of Figure 6, we show the integrated charge asymmetries A_C^y at the Tevatron (solid green curve) and $A_C^{|y|}$ at the LHC8 (solid black curve) as functions of a lower cut on the jet transverse momentum, $p_T^{j,\min}$. At the Tevatron, little phase space is available for the production of a hard jet. The integrated charge asymmetry is dominated by the region of low p_T^j , i.e. by its behavior in the collinear limit. A stronger cut on p_T^j therefore increases A_C^y by several percent with respect to the result based on the detector cut $p_T^{j,\min} = 20$ GeV. At the LHC, where the phase space for the jet is larger, the high- p_T^j regime is more important. We observe that already for $p_T^{j,\min} \geq 15$ GeV the asymmetry starts to decrease with increasing $p_T^{j,\min}$. It is thus desirable to aim at keeping the experimental cut on p_T^j as low as possible, in order not to suppress the charge asymmetry. In practice, the cut on p_T^j is always accompanied by the above-mentioned cut on the jet rapidity $|y_j|$. We display the effect of the detector cuts $|y_j| \leq 2$ for the Tevatron (dashed green curve) and $|y_j| \leq 2.5$ for the LHC (dashed black curve), which increase the charge asymmetry in particular in the region of small $p_T^{j,\text{cut}}$. The dependence of the asymmetries on a p_T^j cut is thus dampened at the Tevatron, but strengthened at the LHC by the detector cut on $|y_j|$.

3 Charge asymmetry from massive color-octet bosons

Massive color-octet vector bosons are expected to leave significant imprints on top-quark pair production at hadron colliders. Such “massive gluons” arise, for instance, as witnesses of an enlarged gauge symmetry $SU(3)_L \times SU(3)_R$ at higher energies as in models with chiral color [33] or topcolor [34], or as Kaluza-Klein excitations of the QCD gluon from compactified extra dimensions. Generically, the interactions of massive gluons with SM particles relevant for

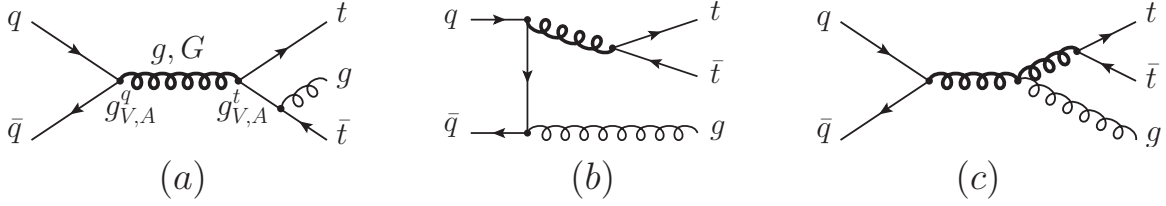


Figure 7: Leading contributions to the process $q\bar{q} \rightarrow t\bar{t}g$ from color-octet vector bosons (bold curled lines) with vector couplings $g_V^{q,t}$ and axial-vector couplings $g_A^{q,t}$ to quarks. Diagrams for $qg \rightarrow t\bar{t}q$ are obtained by crossing $\bar{q} \leftrightarrow g$. Diagrams with interchanged $t \leftrightarrow \bar{t}$ in (a) and $q \leftrightarrow \bar{q}$ in (b) are not shown.

top-antitop production are determined by the following Lagrangian,

$$\mathcal{L} = -ig_s \bar{q}_i \gamma^\mu G_\mu^a T^a [g_V^i + \gamma_5 g_A^i] q_i - g_s f_{abc} [(\partial_\mu G_\nu^a - \partial_\nu G_\mu^a) G^{b\mu} g^{c\nu} + G^{a\mu} G^{b\nu} (\partial_\mu g_\nu^c)], \quad (13)$$

where g_μ^a and G_μ^a denote the QCD gluon and massive gluon fields; T^a and f_{abc} are the generators and structure constants of the $SU(3)_C$ gauge group of strong interactions; and g_V^i and g_A^i describe the vector (V) and axial-vector (A) couplings of the massive gluon to quarks with flavor i in their weak eigenstates. If the triple gauge boson coupling in (13) arises from gauge-kinetic terms, its strength is fixed by the QCD coupling constant g_s (see also [35]). Gauge invariance further prohibits the coupling of two gluons to an uneven number of massive gluons.⁸ The production of a single color-octet vector boson via gluon-gluon fusion is therefore suppressed with respect to quark-antiquark annihilation.

In this section, we investigate the effects of massive gluons in $t\bar{t} + j$ production at the LHC. The generation of a charge asymmetry from vector and axial-vector contributions is explained in detail. We discuss strategic cuts that enhance massive gluon effects on $A_C^{|y|}$. We further show that the angular distribution of the jet contains information that can be used to distinguish between vector and axial-vector couplings. In our numerical studies, we employ the same inputs and cuts on the jet properties as for the QCD analysis, which were given in Section 2.1.

3.1 Charge-asymmetric vector and axial-vector contributions

Massive gluon contributions to the charge-symmetric and -antisymmetric $t\bar{t} + j$ cross section arise from their interference with the QCD amplitude, $g - G$ ($\sigma_{s,a}^{gG}$), as well as through interference with themselves, $G - G$ ($\sigma_{s,a}^G$). They contribute to the top-quark charge asymmetry at the LHC, yielding

$$A_C^{|y|,\text{tot}} = \frac{\sigma_a^g + \sigma_a^{gG} + \sigma_a^G}{\sigma_s^g + \sigma_s^{gG} + \sigma_s^G} \equiv A_C^{|y|,\text{SM}} + \Delta A_C^{|y|}, \quad \text{with } A_C^{|y|,\text{SM}} = \frac{\sigma_a^g}{\sigma_s^g}. \quad (14)$$

⁸This argument holds for models with an enlarged gauge symmetry. In warped extra dimensions, the ggG vertex vanishes due to the wave function orthogonality of the gluon and its Kaluza-Klein excitations [36].

	σ_s^g	σ_s^{gG}	σ_s^G	σ_a^g	σ_a^{gG}	σ_a^G
$(a) - (a), (b) - (b)$	1	$g_V^q g_V^t$	$(g_{V,A}^q)^2 (g_{V,A}^t)^2$	—	$g_A^q g_A^t$	$g_V^q g_V^t g_A^q g_A^t$
$(a) - (b) : f_{abc}^2$	1	$g_V^q g_V^t$	$(g_{V,A}^q)^2 (g_{V,A}^t)^2$	—	$g_A^q g_A^t$	$g_V^q g_V^t g_A^q g_A^t$
$(a) - (b) : d_{abc}^2$	—	$g_A^q g_A^t$	$g_V^q g_V^t g_A^q g_A^t$	1	$g_V^q g_V^t$	$(g_{V,A}^q)^2 (g_{V,A}^t)^2$
$(c) - (a), (c) - (b)$	1	$g_V^q g_V^t$	$(g_{V,A}^q)^2 (g_{V,A}^t)^2$	—	$g_A^q g_A^t$	$g_V^q g_V^t g_A^q g_A^t$
$(c) - (c)$	1	$g_V^q g_V^t$	$(g_{V,A}^q)^2 (g_{V,A}^t)^2$	—	$g_A^q g_A^t$	$g_V^q g_V^t g_A^q g_A^t$

Table 3: Contributions to $t\bar{t} + j$ production from $g - g$ interference ($\sigma_{s,a}^g$), $g - G$ interference ($\sigma_{s,a}^{gG}$), and $G - G$ interference ($\sigma_{s,a}^G$). Contributions labeled $(a) - (b)$ etc. correspond to interfering diagrams in Figure 7 with gluon (g) and massive gluon (G) insertions. Leading massive gluon effects in inclusive $t\bar{t}$ production follow the pattern of the first line.

The charge asymmetry in $t\bar{t} + j$ production is generated at LO by the interference of the diagrams shown in Figure 7. To calculate the contributions to $\sigma_{s,a}^{gG}$ and $\sigma_{s,a}^G$, we use the Feynman rules from [35] and work in the unitary gauge. Notice that the cancellation of unphysical gluon polarization modes requires the inclusion of the diagram (c) with two massive gluons, even though its contribution is suppressed by $\mathcal{O}(M_G^{-2})$ with respect to the diagrams (a) and (b).

Let us discuss the sources of a charge asymmetry from massive gluons in $t\bar{t} + j$ production in detail. First we focus on the interference of initial- (ISR) and final-state radiation (FSR), i.e., the interference of diagrams (a) and (b) in Figure 7. Disregarding the color structure, the amplitudes from $V - V$ or $A - A$ (from $V - A$) interference are antisymmetric (symmetric) under $t \leftrightarrow \bar{t}$. The color structure of ISR-FSR interference can be decomposed in terms of a symmetric factor $d_{abc} = 2 \text{Tr}[\{T^a, T^b\}T^c]$ and an antisymmetric factor $f_{abc} = -2i \text{Tr}[[T^a, T^b]T^c]$. A charge asymmetry can thus be generated in two ways: firstly, from $V - V$ or $A - A$ interference paired with a symmetric color structure d_{abc}^2 , or secondly by $V - A$ interference and an antisymmetric color structure f_{abc}^2 . In QCD, the asymmetry is generated by the (antisymmetric) ISR-FSR interference of two vector currents ($g - g$) and is proportional to the symmetric color factor d_{abc}^2 [37]. Therefore, the first mechanism is at work. A massive gluon with pure V couplings generates an asymmetry by the same mechanism as in QCD. A massive color octet with A couplings, dubbed axigluon, contributes to the charge asymmetry via both mechanisms. When interfering with itself, the asymmetry is generated via the first mechanism, i.e. by the antisymmetric amplitude. When interfering with the QCD gluon or a massive color octet with V couplings, the second mechanism applies and the antisymmetric color structure is the source of the asymmetry. Besides ISR-FSR interference, a charge asymmetry can be generated from all remaining combinations of diagrams in Figure 7 through the interference of a V and an A current. The additional emitted gluon is just a “spectator” of the asymmetry generated by the $V - A$ interference. The various contributions to the charge-symmetric and -asymmetric cross sections σ_s and σ_a are summarized in Table 3. Contributions proportional to $g_V^m g_A^n$ with

$mn = 11, 13, 31$ are omitted in the table, but taken into account in our numerical analysis. Their contribution to σ_s and σ_a is negligibly small. Contributions from the channels $q\bar{q} \rightarrow t\bar{t}g$ and $qg \rightarrow t\bar{t}q$ exhibit the same behavior in terms of quark couplings $g_{V,A}^{q,t}$, albeit with different kinematic coefficients.

Results for the contributions to the charge asymmetry from ISR-FSR interference, labeled (a) – (b) in lines two and three of Table 3, have been previously obtained in [25]. Our results agree with the analytic expressions given in the appendix therein. In our analysis, we calculated the complete set of massive gluon contributions to hadronic $t\bar{t} + j$ production. The analytic results can be readily obtained from the authors.

3.2 Benchmark scenarios

To estimate the effects of massive gluons on the charge asymmetry in $t\bar{t} + j$ production at the LHC, we define a set of benchmark points given in Table 4. The mass of the color octet is set to $M_G = 2 \text{ TeV}$, and its width Γ_G is fixed by assuming the decay to SM fermions only (see (47) in [40]). We distinguish between scenarios with V and A couplings to quarks. The couplings to light quarks $g_{V,A}^q$ are suppressed in order to respect the bounds from dijet resonance searches at the LHC [38, 39]. For the scenarios VA^{xy} of massive gluons with both V and A couplings to quarks, the magnitude is chosen such that the combination $(g_V^{q,t})^2 + (g_A^{q,t})^2$ is (almost) the same as for the scenarios V^x, A^x . Constraints from dijet and $t\bar{t}$ resonance searches [5, 6, 7, 8], which are mostly sensitive to this combination of couplings, are thereby likewise respected. Scenarios with different signs of $g_{V,A}^q \cdot g_{V,A}^t$, marked accordingly by an index + or –, probe positive and negative interference with the QCD amplitude, i.e. the sign of $\sigma_{s,a}^{gG}$ in Table 3. In the case of both V and A couplings, we define a third scenario VA^{+-} , which probes in addition the sign of the $G - G$ interference terms $\sigma_{s,a}^G$. Scenarios with VA structures arise naturally from models with chiral couplings. In particular, a massive gluon that couples only to right-handed (left-handed) quarks yields same-sign (opposite-sign) couplings g_V and g_A , as implemented in $VA^{\pm\pm}$ (VA^{+-}). All benchmarks are in agreement with the current bounds from charge-symmetric observables at the Tevatron and the LHC [40]. Benchmarks with axial-vector couplings, in particular A^- and $VA^{\pm-}$, offer in addition an explanation of the enhanced forward-backward asymmetry measured at the Tevatron [41]. Massive gluons lighter than 2 TeV are strongly constrained by the above-mentioned observables, as well as by measurements of the invariant mass spectrum of $t\bar{t}$ production at the Tevatron and the LHC [42, 43, 44]. Those constraints can only be relaxed, if the couplings to both light quarks and top quarks, $g_{V,A}^q$ and $g_{V,A}^t$, are strongly suppressed and if the width Γ_G is large [45]. Light massive gluons will not be considered in this analysis.

3.3 Massive gluons effects close to the resonance

As in QCD, contributions from massive gluons to the LHC asymmetry are suppressed by the large symmetric gg background entering the normalization of $A_C^{|y|}$. Massive gluon effects are further suppressed, because the average partonic CM energy in $t\bar{t} + j$ production at LHC8 is as low as $\sqrt{\hat{s}} \approx 500 \text{ GeV}$. This is well below the resonance region of $\sqrt{\hat{s}} \approx 2 \text{ TeV} = M_G$, where massive gluons could yield large effects. Effects on the total asymmetry $A_C^{|y|}$ in $t\bar{t} + j$

$M_G = 2 \text{ TeV}$	V^+	V^-	A^+	A^-	VA^{++}	VA^{--}	VA^{+-}
g_V^q	0.5	0.5	0	0	0.35	0.35	0.35
g_V^t	2	-2	0	0	1.5	-1.5	1.5
g_A^q	0	0	0.5	0.5	0.35	0.35	0.35
g_A^t	0	0	2	-2	1.5	-1.5	-1.5
$\Gamma_G/M_G [\%]$	17.7	17.7	17.3	17.3	19.4	19.4	19.4

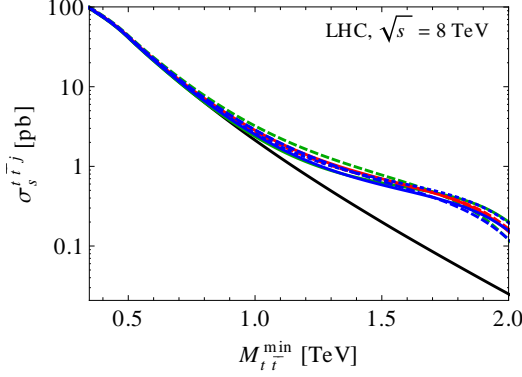
Table 4: Benchmark points for massive gluons in $t\bar{t} + j$ production. Benchmarks are labeled X^{sgn} , where $X = V, A, VA$ stands for vector, axial-vector or both couplings to quarks, and $\text{sgn} = \pm$ refers to the sign of the product $g_{V,A}^q \cdot g_{V,A}^t$. All scenarios respect the constraints from Tevatron and LHC measurements.

production at the LHC are therefore small, if no cuts are applied. In the following, we will discuss how the kinematic cuts defined in Section 2.1 can enhance the charge asymmetry from massive gluons.

The suppression due to the gg background, as already described in Section 2.1, is relieved by selecting events with a large boost along the beam line. A lower cut on the total rapidity $y_{t\bar{t}j}$ projects on the (boosted) $q\bar{q}$ and qg initial states. Both QCD and massive gluon contributions to the charge-asymmetric cross section σ_a are thereby enhanced with respect to the production cross section σ_s . The enhancement of $A_C^{|y|}$ through a cut on $y_{t\bar{t}j}$ is largely independent from the massive gluon properties, up to a subleading effect on σ_s that enters the normalization and differs for V or A couplings to quarks.

An efficient way to increase massive gluon effects on $A_C^{|y|}$ is to apply a lower cut on the top-antitop invariant mass $M_{t\bar{t}}$. This enhances the partonic CM energy and brings it closer to the region $M_{t\bar{t}} \approx M_G$, where massive gluons are produced on shell. The $M_{t\bar{t}}$ spectrum of the asymmetry is highly model-dependent and sensitive to the interplay of $g - G$ and $G - G$ interference effects. In Figures 8 and 9, we show the effects of massive gluons on the symmetric cross section and on the charge asymmetry, $\Delta A_C^{|y|}$ defined in (14), at LHC8 as a function of a lower cut on the invariant mass, $M_{t\bar{t}}^{\text{min}}$. Massive gluon contributions are displayed for the seven benchmark points defined in Table 4. In the symmetric cross section σ_s (Figure 8), resonance effects of massive gluons show up in the tail of the $M_{t\bar{t}}$ spectrum. They are largely independent from the respective couplings to quarks. Close to the resonance region, the massive gluon contribution is dominated by σ_s^G (cf. Table 3), which in large part does not distinguish between V and A couplings.

The charge asymmetry $A_C^{|y|}$ (Figure 9), in turn, is well suited to disentangle massive gluon contributions. For moderate cuts on $M_{t\bar{t}}$, the effects of pure V or A couplings are driven by the interference with QCD, σ_a^{gG} . An axigluon with same-sign couplings to light quarks and top quarks (A^+ , solid red curve) interferes constructively with QCD, yielding a negative asymmetry. An axigluon with opposite-sign couplings (A^- , dashed red curve) interferes destructively and generates a positive asymmetry. Vector contributions (green curves) to σ_a^{gG} are much smaller in magnitude and of opposite sign with respect to axial-vector ones. In scenarios with both V and A couplings (blue curves), the interference term σ_a^{gG} can be of either



$M_{t\bar{t}}^{\min} = 1 \text{ TeV}$	$\sigma_s^{\text{tot}}/\sigma_s^g - 1$	$\Delta A_C^{[y]} [\%]$
V^+, V^-	0.11, 0.51	-0.22, -2.3
A^+, A^-	0.33, 0.27	-6.7, +4.3
VA^{++}	0.18	+5.4
VA^{--}	0.35	+8.9
VA^{+-}	0.23	-6.9

Figure 8: Left: Massive gluon contributions to the charge-symmetric cross section $\sigma_s^{t\bar{t}j}$ at LHC8 with a lower cut on the invariant mass, $M_{t\bar{t}}^{\min}$, for all benchmarks from Table 4 (colored as in Figure 9). The QCD cross section (black curve) is displayed at LO. Cuts on the jet kinematics $p_T^j \geq 25 \text{ GeV}$ and $|y_j| \leq 2.5$ are applied. Right: Massive gluon effects on $\sigma_s^{t\bar{t}j}$ and $A_C^{[y],t\bar{t}j}$ for $M_{t\bar{t}}^{\min} = 1 \text{ TeV}$ and the benchmarks from Table 4.

sign, depending on the dominance and flavor dependence of V or A contributions. Those VA scenarios feature additional contributions to σ_a^G , which are large both in the resonance region and closer to the top-pair production threshold. They are typically positive, but can be negative if V and A couplings to light quarks or top quarks are of opposite sign, as is realized in the benchmark VA^{+-} (dotted blue curve). In all scenarios, the interference term changes its sign at $M_{t\bar{t}}^{\min} = 1.72 \text{ TeV}$, such that the massive gluon contribution is completely determined by σ_a^G . The dominance of VA contributions to σ_a^G in this region is apparent when comparing with pure V or A contributions. In the latter case, one finds $\Delta A_C^{[y]} = -4\%$ for the scenarios V^\pm, A^\pm , which is exceeded by the much larger contribution of $\Delta A_C^{[y]} = +29\%$ (-31%) for the scenarios $VA^{\pm\pm}$ (VA^{+-}). In the table in Figure 8, we give results for massive gluon contributions to the cross section $\sigma_s^{\text{tot}} = \sigma_s^g + \sigma_s^{gG} + \sigma_s^G$ and the charge asymmetry $A_C^{[y]}$ for $M_{t\bar{t}}^{\min} = 1 \text{ TeV}$. They illustrate once more that the cross section can be significantly enhanced in all massive gluon scenarios at high $M_{t\bar{t}}$, and that contributions to the charge asymmetry are sizeable and strongly model-dependent.

The total LHC asymmetry $A_C^{[y],\text{tot}}$ is obtained by adding the QCD asymmetry $A_C^{[y],\text{SM}}$ to the massive gluon effects $\Delta A_C^{[y]}$ shown in Figure 9. As we saw in Section 2.4, the QCD asymmetry at LO is small and negative and increases slightly at high $M_{t\bar{t}}$. For $M_{t\bar{t}}^{\min} \leq 1 \text{ TeV}$, $A_C^{[y],\text{SM}}$ stays below -1.5% and does not exceed $A_C^{[y],\text{SM}} = -2.5\%$ for even stronger cuts on $M_{t\bar{t}}$, as can be observed from Figure 6, left. Furthermore, NLO corrections decrease the absolute value of the QCD asymmetry. In the region of high $M_{t\bar{t}}$, the total asymmetry is thus dominated by massive gluon effects, $A_C^{[y],\text{tot}} \approx \Delta A_C^{[y]}$, and can be read off to a good approximation from Figure 9.

Since the $M_{t\bar{t}}$ spectrum of the asymmetry nicely resolves the various contributions, we take the opportunity to compare massive gluon effects on the charge asymmetries in exclusive $t\bar{t} + j$ production, $A_C^{[y],t\bar{t}j}$ (Figure 9), and in inclusive $t\bar{t}$ production, $A_C^{[y],t\bar{t}}$ (Figure 10,

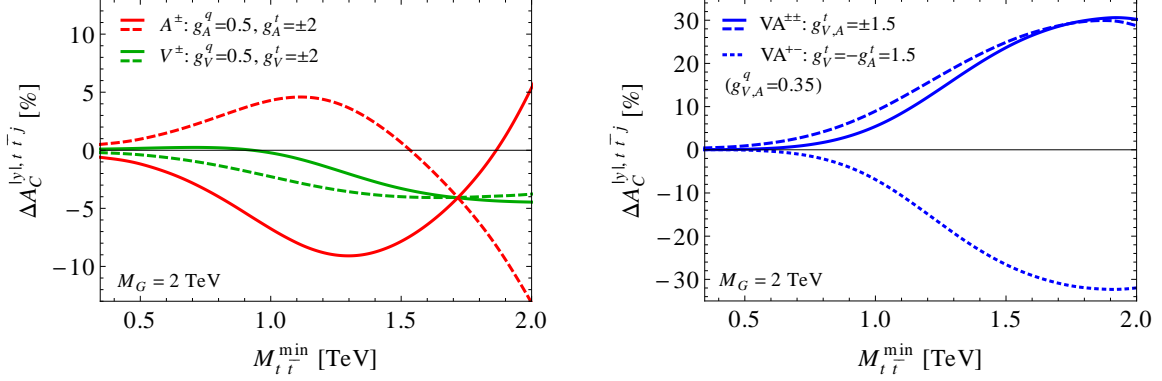


Figure 9: Massive gluon contributions to the exclusive charge asymmetry $A_C^{[y], t\bar{t}j}$ at LHC8 with a lower cut $M_{t\bar{t}}^{\min}$ for the benchmark scenarios defined in Table 4.

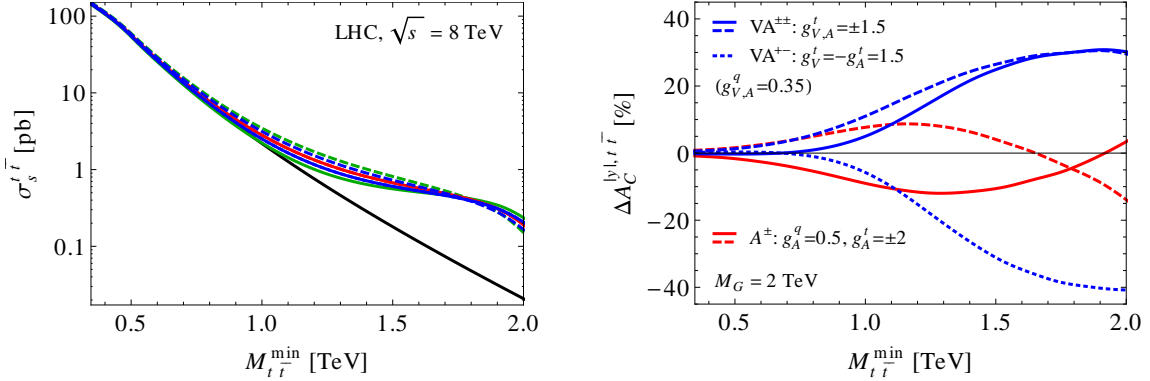


Figure 10: Massive gluon contributions to the cross section $\sigma_s^{t\bar{t}}$ (left) and to the charge asymmetry $A_C^{[y], t\bar{t}}$ (right) in inclusive $t\bar{t}$ production at LHC8 for the benchmarks defined in Table 4.

right panel). The inclusive asymmetry $A_C^{[y], t\bar{t}}$ is generated at tree level by the interference of an axigluon with the QCD gluon; all leading effects follow the pattern in the first line of Table 3. Charge-asymmetric contributions from massive gluons with V couplings are absent in inclusive $t\bar{t}$ production at LO and can thus be probed only in the exclusive asymmetry $A_C^{[y], t\bar{t}j}$. Axial-vector contributions to $A_C^{[y], t\bar{t}}$ and $A_C^{[y], t\bar{t}j}$ are of similar size, but they arise from different sources. In inclusive $t\bar{t}$ production, the LO asymmetry is generated solely by $V - A$ interference. In $t\bar{t} + j$ production, the same mechanism is at work for ISR-ISR and FSR-FSR interference terms (Table 3, line 1), which are NLO corrections to the inclusive asymmetry. The dominant contribution, however, stems from ISR-FSR interference (Table 3, line 2), where the asymmetry is generated by the antisymmetric color structure. Both contributions interfere destructively, which reduces the total effect on $A_C^{[y], t\bar{t}j}$. In the search for massive color octets, the charge asymmetry in $t\bar{t} + j$ production has thus more to offer than NLO corrections to the inclusive asymmetry. It additionally probes vector couplings at tree level and effects from diagrammatically different sources.

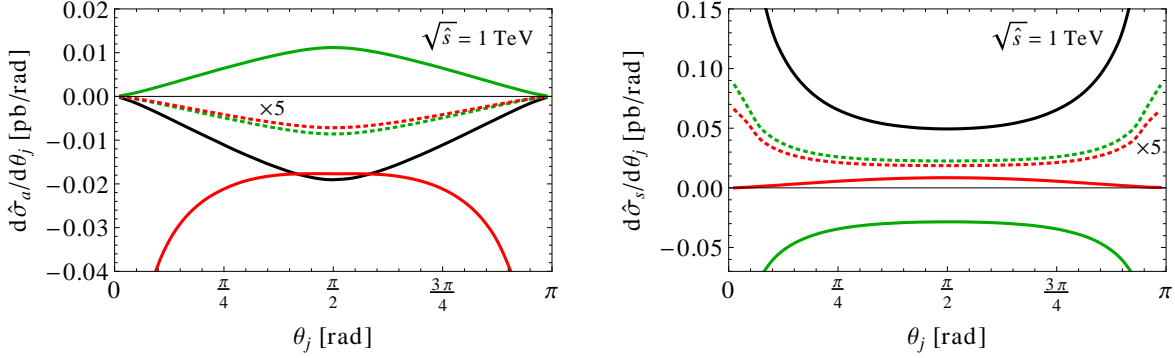


Figure 11: Jet angular distribution of the charge-asymmetric (left) and -symmetric (right) partonic $q\bar{q} \rightarrow t\bar{t}g$ cross sections for $\sqrt{\hat{s}} = 1$ TeV and $p_T^j \geq 2$ GeV. Shown are contributions from QCD (black), as well as from $g - G$ (solid) and $G - G$ (dotted, rescaled by a factor 5) interference for the massive gluon benchmarks V^+ (green) and A^+ (red) defined in Table 4.

3.4 Massive gluon couplings from the jet angular distribution

The angular distribution of the jet in $t\bar{t} + j$ production provides complementary information on the massive gluon couplings to the invariant mass spectrum. Like in QCD, the shape of the jet distribution for massive gluon contributions is driven by the behavior of the cross sections in the collinear regime. Figure 11 shows the jet angular distributions $d\hat{\sigma}_a/d\theta_j$ (left) and $d\hat{\sigma}_s/d\theta_j$ (right) defined in (11) for the partonic process $q\bar{q} \rightarrow t\bar{t}g$ at a CM energy of $\sqrt{\hat{s}} = 1$ TeV. For $V - V$ interference (solid and dashed green curves) and $A - A$ interference (dashed red curve), the collinear behavior follows that of QCD (black curve). The symmetric cross section σ_s exhibits a collinear divergence, whereas the asymmetric cross section σ_a smoothly vanishes in the collinear limit. For $V - A$ interference (solid red curve), the collinear behavior is reversed with respect to QCD: σ_s vanishes in the collinear limit and σ_a is divergent. In short, only those amplitudes for which the jet determines the properties under charge conjugation (disregarding the color structure) are finite in the collinear limit. From a diagrammatic point of view, only ISR-FSR interference is collinear finite and generates a central jet. All other contributions are collinear divergent, so that the jet is preferentially emitted in the beam direction.

The jet angular distribution may serve as a tool to distinguish V from A contributions to the charge asymmetry by exploring their differing collinear behavior. In Figure 12, the LHC asymmetry $A_C^{|y|, \text{tot}}$ (left), defined in (14), and the cross section σ_s^{tot} (right) are shown as a function of the rapidity \hat{y}_j for a lower cut on the invariant mass, $M_{t\bar{t}} \geq 1$ TeV. For massive gluons with vector couplings (green curve), just as in QCD (black curve), the asymmetry reaches its maximum in the central jet region. The vector contribution slightly increases the maximal asymmetry from $A_C^{|y|}(\hat{y}_j = 0) = -3.7\%$ in QCD to $A_C^{|y|}(\hat{y}_j = 0) = -4.0\%$. For axial-vector contributions, the shape of the jet distribution is driven by the interplay of QCD and axigluon terms. In the central region, the asymmetry exhibits a maximum of $A_C^{|y|}(\hat{y}_j = 0) = -12.4\%$, because σ_a^{tot} is large and negative, while σ_s^{tot} is in its minimum and increases for more forward-emitted jets (cf. Figure 11). A second maximum is obtained in

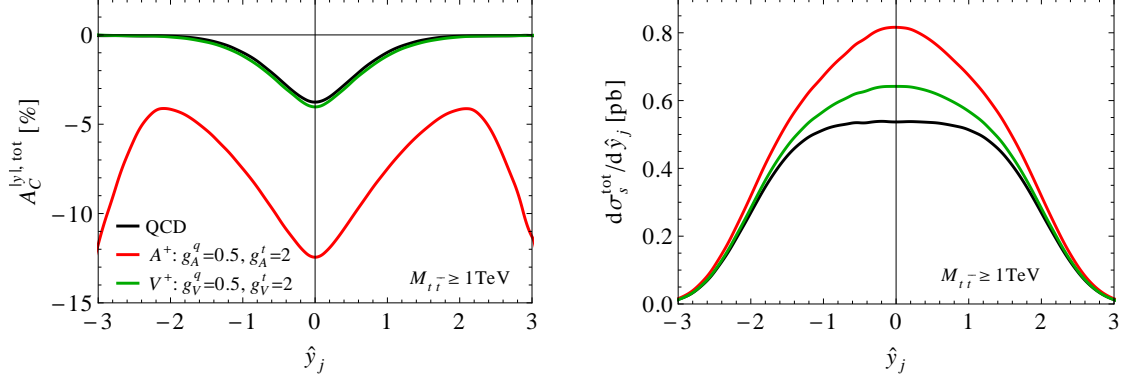


Figure 12: Charge asymmetry $A_C^{|y|, \text{tot}}$ (left) and differential cross section $d\sigma_s^{\text{tot}}/d\hat{y}_j$ (right) at LHC8 as a function of the rapidity \hat{y}_j for $M_{t\bar{t}} \geq 1 \text{ TeV}$. Shown is the sum of QCD and massive gluon contributions for the scenarios V^+ (green) and A^+ (red).

the limit of large $|\hat{y}_j|$, where the collinear enhancement of the axigluon-QCD interference term σ_a^{gG} dominates the asymmetry. The appearance of a large charge asymmetry in the forward-jet region is thus a clear signal of axial-vector contributions in $t\bar{t} + j$ production. Again, a reliable numerical prediction of the observables in this region requires a dedicated study of resummation effects in the collinear limit.

4 Conclusions

In this work, we have investigated the charge asymmetry in $t\bar{t} + j$ production for the Tevatron and LHC observables. Jet kinematics of the total cross section and of the charge asymmetry have been explored in detail in terms of the jet energy E_j and the scattering angle θ_j . The jet angular distribution is driven by the behavior of the cross sections σ_s and σ_a in the collinear limit. In QCD, the charge-asymmetric cross section σ_a does not exhibit a logarithmic enhancement in the limit $\theta_j \rightarrow 0$ and reaches its maximum if the jet is emitted perpendicular to the beam axis. This is also the region where the symmetric cross section σ_s , which normalizes the charge asymmetry and does exhibit a collinear divergence, is less affected by resummation effects. The utility of a selection of central jet emission is thus twofold: It enhances the charge asymmetry A_C and simultaneously yields a collinear-safe observable. The dependence of the charge asymmetry on the jet energy is mild, apart from the region of large E_j , where A_C is suppressed.

These considerations for the jet kinematics can be applied to the charge asymmetries both at the Tevatron and at the LHC. At the Tevatron, the charge asymmetry in QCD at LO is sizeable, $A_C^y = -12.6\%$, but reduced to $A_C^y \approx -4\%$ by NLO corrections. We found that in the central jet region, the asymmetry is as large as $A_C^y(\hat{y}_j = 0) = -27\%$. An upper cut on the jet rapidity in the parton frame, $\hat{y}_j = y_j - y_{t\bar{t}j}$, is thus suited to enhance the integrated asymmetry. Apart from jet kinematics, the charge asymmetry is sensitive to the top-antitop rapidity difference Δy , which defines the observable A_C^y , and to a lesser extent to the invariant

mass $M_{t\bar{t}}$. Lower cuts on those variables can further enhance the asymmetry, at the cost of strongly reducing the cross section σ_s . Since the phase space of hard jet emission in $t\bar{t}$ production at the Tevatron is small, the cross section for $t\bar{t} + j$ production amounts only to $\sigma_s^{\text{LO}} = 1.42 \text{ pb}$. From an experimental point of view, the application of cuts that reduce the cross section is therefore not welcome, and the measurement of the total charge asymmetry with the full data set of 10 fb^{-1} luminosity is difficult.

At the LHC, the phase space in $t\bar{t}$ production and thereby cross section for hard jet emission is much larger due to the high CM energy. At $\sqrt{s} = 8 \text{ TeV}$, the cross section is sizeable, $\sigma_s^{\text{LO}} = 97.5 \text{ pb}$, but the total charge asymmetry $A_C^{|y|} = -0.56 \%$ is tiny due to the large charge-symmetric gg background. This background can be suppressed by selecting $t\bar{t} + j$ events with a large boost β of the partonic CM frame, which predominantly stem from $q\bar{q}$ or gg initial states. A lower cut on the correlated lab-frame rapidity $y_{t\bar{t}j}$, for instance $|y_{t\bar{t}j}| \geq 1$, enhances the charge asymmetry by a factor of three to $A_C^{|y|} = -1.62 \%$ and simultaneously reduces the cross section to $\sigma_s = 19.2 \text{ pb}$. The charge asymmetry exhibits a similar sensitivity to jet kinematics for moderate cuts. The maximal asymmetry is reached in the central jet region, $A_C^{|y|}(\hat{y}_j = 0) = -1.5 \%$. A third possibility to increase the charge asymmetry is via a lower cut on the difference of absolute top and antitop rapidities $|\Delta|y|$, which defines the LHC observable $A_C^{|y|}$. Since the cross section of $t\bar{t} + j$ production at the LHC is sizeable and the data sample for LHC8 is expected to reach about 20 fb^{-1} in 2012, the application of cuts is possible and indispensable in order to obtain a measurable charge asymmetry. We showed that by combining cuts on three suitable variables, for $|y_{t\bar{t}j}| \geq 1$, $|\hat{y}_j| \leq 0.5$ and $|\Delta|y| \geq 0.5$ the asymmetry can be enhanced to $A_C^{|y|} = -4.0 \%$ with $\sigma_s = 4.0 \text{ pb}$. An asymmetry of that size and for a comparable cross section cannot be obtained by applying a stronger cut on only one of the variables. However, even for stronger combined cuts the asymmetry at LHC8 hardly exceeds -5% , making its measurement a challenging task.

Massive color-octet bosons, in turn, can generate large effects on the charge asymmetry at the LHC. Both vector and axial-vector couplings contribute to $A_C^{|y|}$ at tree level. An asymmetry from massive gluons with vector couplings to quarks arises just as in QCD from the antisymmetric amplitude for the ISR-FSR interference of two vector currents. With axial-vector couplings, an asymmetry from axigluon-gluon interference can be generated either by the antisymmetric amplitude for ISR-ISR or FSR-FSR interference or by the antisymmetric color structure in the case of ISR-FSR interference. The different contributions from vector and axial-vector couplings can be disentangled after applying a lower cut on the invariant mass, which projects on the resonance region $M_{t\bar{t}} \approx M_G$, where massive gluon effects are maximal. Contributions from axigluons are generically larger than from massive gluons with vector couplings and depend on the respective sign of the couplings to light quarks and top quarks. For $M_{t\bar{t}}^{\text{min}} = 1 \text{ TeV}$, they amount to $\Delta A_C^{|y|} = -6.7 \%, +4.3 \%, -0.22 \%, -2.3 \%$ for the respective benchmark scenarios A^+, A^-, V^+ and V^- defined in Table 4. The effects are mostly driven by the QCD-massive gluon interference term σ_a^{gG} . At high $M_{t\bar{t}}$, the massive-gluon term σ_a^G yields large effects, if both vector and axial-vector couplings (i.e. chiral couplings) are present. Contributions to the charge asymmetry for $M_{t\bar{t}}^{\text{min}} = 1.72 \text{ TeV}$, where σ_a^{gG} vanishes, can be as large as $\Delta A_C^{|y|} = +29 \%$ or -31% for the benchmarks $VA^{\pm\pm}$ or VA^{+-} . Thus, if the charge asymmetry is enhanced by an axial-vector or a chiral massive gluon contribution, it

should be observable at the LHC. The jet angular distribution can be used to obtain further information about the vector or axial-vector nature of massive gluon couplings. The differing collinear behavior of the cross sections allows to distinguish axigluon effects from QCD and other vector contributions. An axigluon generates a second maximum of $A_C^{|y|}$ in the forward-jet region, in addition to the common maximum for central jets. In order to exploit this information, however, a dedicated study of the collinear enhancement and a good experimental control of the measurement in the forward region are necessary.

At the full power of the LHC, $\sqrt{s} = 14$ TeV, the integrated charge asymmetry is smaller than at $\sqrt{s} = 8$ TeV due to the increased gg background. However, since the cross section for $t\bar{t} + j$ production is larger, stronger cuts can be applied. We found that the resulting charge asymmetry $A_C^{|y|}$ in QCD can be of the same size or larger than at LHC8 for comparable cross sections. For massive gluon searches, LHC14 can be a convenient setup because the large CM energy allows to produce very heavy such particles. LHC14 is therefore not disfavored to explore a charge asymmetry both in QCD and from massive gluons, and might be even more successful than LHC8 in the search for heavy resonances.

We conclude that the charge asymmetry in $t\bar{t} + j$ production provides an interesting playground for tests of QCD and of physics beyond the SM in top-quark pair production. The jet angular distribution serves as a useful tool to explore the kinematic features of the final state on top of those in inclusive $t\bar{t}$ production. The smallness of the QCD charge asymmetry in $t\bar{t} + j$ production at the LHC is a challenge for future measurements. In turn, it makes $A_C^{|y|}$ a clean observable to test the properties of new particles via charge conjugation. The year of the top quark is in its full bloom. Top-quark physics beyond inclusive $t\bar{t}$ production at the LHC is in its infancy, but will soon be testable in more detail.

5 Acknowledgements

It is our pleasure to thank Lucia Masetti, Andreas von Manteuffel, Ben Pecjak and Hubert Spiesberger for helpful discussions and Stefan Weinzierl for comments on the manuscript. The work of S. B. is supported by the Initiative and Networking Fund of the Helmholtz Association, contract HA-101 (‘Physics at the Terascale’) and by the Research Center ‘Elementary Forces and Mathematical Foundations’ of the Johannes Gutenberg-Universität Mainz.

A Phase space kinematics for $t\bar{t} + j$ production

We parameterize the momenta of the initial-state hadrons by $P_1 = \sqrt{s}/2(x_1, 0, 0, x_1)$ and $P_2 = \sqrt{s}/2(x_2, 0, 0, -x_2)$. The boost β of the partonic CM frame with respect to the lab frame can then be expressed in terms of the parton momentum fractions x_1 and x_2 as ⁹

$$\beta = \frac{p_t^z + p_{\bar{t}}^z + p_j^z}{E_t + E_{\bar{t}} + E_j} = \frac{P_1^z + P_2^z}{P_1^0 + P_2^0} = \frac{x_1 - x_2}{x_1 + x_2}, \quad -1 < \beta < 1. \quad (15)$$

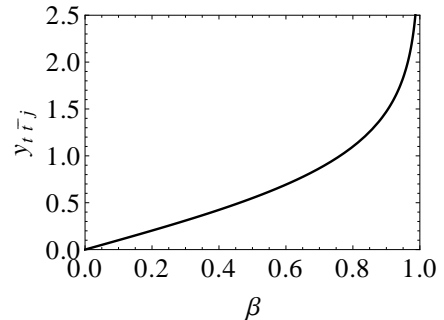
⁹Here, all momenta and energies are defined in the lab frame. The z axis coincides with the direction of the incoming hadron with momentum P_1 .

Experimentally, the boost of the partonic CM frame can be determined by measuring the rapidity of the $t\bar{t} + j$ system in the lab frame, $y_{t\bar{t}j}$.

Both quantities are related via

$$y_{t\bar{t}j} = \frac{1}{2} \ln \frac{\sum_{i=t,\bar{t},j} (E_i + p_i^z)}{\sum_{i=t,\bar{t},j} (E_i - p_i^z)} \quad (16)$$

$$\stackrel{\text{LO}}{=} \frac{1}{2} \ln \frac{x_1}{x_2} = \frac{1}{2} \ln \frac{1 + \beta}{1 - \beta}.$$



A lower cut on the rapidity $y_{t\bar{t}j}$ in the lab frame therefore directly translates into a selection of events with a higher boost β .

References

- [1] G. Aad *et al.* [ATLAS Collaboration], ATLAS-CONF-2012-024.
- [2] S. Chatrchyan *et al.* [CMS Collaboration], CMS-PAS-TOP-12-007.
- [3] U. Langenfeld, S. Moch and P. Uwer, Phys. Rev. D **80**, 054009 (2009) [arXiv:0906.5273 [hep-ph]].
- [4] V. Ahrens, A. Ferroglia, M. Neubert, B. D. Pecjak and L. L. Yang, Phys. Lett. B **703**, 135 (2011) [arXiv:1105.5824 [hep-ph]].
- [5] T. Aaltonen *et al.* [CDF Collaboration], Phys. Rev. D **84**, 072004 (2011) [arXiv:1107.5063 [hep-ex]].
- [6] V. M. Abazov *et al.* [D0 Collaboration], Phys. Rev. D **85**, 051101 (2012) [arXiv:1111.1271 [hep-ex]].
- [7] G. Aad *et al.* [ATLAS Collaboration], arXiv:1207.2409 [hep-ex].
- [8] S. Chatrchyan *et al.* [CMS Collaboration], arXiv:1204.2488 [hep-ex].
- [9] T. Aaltonen *et al.* [CDF Collaboration], CDF Public Note 10807 (2012); Phys. Rev. D **83**, 112003 (2011) [arXiv:1101.0034 [hep-ex]]; CDF Public Note 10436 (2011).
- [10] V. M. Abazov *et al.* [D0 Collaboration], Phys. Rev. D **84**, 112005 (2011) [arXiv:1107.4995 [hep-ex]].
- [11] J. H. Kühn and G. Rodrigo, JHEP **1201**, 063 (2012) [arXiv:1109.6830 [hep-ph]].
- [12] V. Ahrens, A. Ferroglia, M. Neubert, B. D. Pecjak and L. L. Yang, Phys. Rev. D **84**, 074004 (2011) [arXiv:1106.6051 [hep-ph]].

- [13] G. Aad *et al.* [ATLAS Collaboration], ATLAS-CONF-2012-057.
- [14] S. Chatrchyan *et al.* [CMS Collaboration], CMS-PAS-TOP-11-030.
- [15] D. L. Rainwater and D. Zeppenfeld, Phys. Rev. D **60**, 113004 (1999) [Erratum-ibid. D **61**, 099901 (2000)] [hep-ph/9906218].
- [16] M. L. Mangano, Eur. Phys. J. C **59**, 373 (2009) [arXiv:0809.1567 [hep-ph]].
- [17] S. Dittmaier, P. Uwer and S. Weinzierl, Phys. Rev. Lett. **98**, 262002 (2007) [hep-ph/0703120 [hep-ph]].
- [18] S. Dittmaier, P. Uwer and S. Weinzierl, Eur. Phys. J. C **59**, 625 (2009) [arXiv:0810.0452 [hep-ph]].
- [19] K. Melnikov and M. Schulze, Nucl. Phys. B **840**, 129 (2010) [arXiv:1004.3284 [hep-ph]].
- [20] G. Aad *et al.* [ATLAS Collaboration], ATLAS-CONF-2012-083.
- [21] K. Melnikov, A. Scharf and M. Schulze, Phys. Rev. D **85**, 054002 (2012) [arXiv:1111.4991 [hep-ph]].
- [22] A. Kardos, C. Papadopoulos and Z. Trocsanyi, Phys. Lett. B **705**, 76 (2011) [arXiv:1101.2672 [hep-ph]].
- [23] S. Alioli, S. Moch and P. Uwer, JHEP **1201**, 137 (2012) [arXiv:1110.5251 [hep-ph]].
- [24] S. Chatrchyan *et al.* [CMS Collaboration], arXiv:1206.3921 [hep-ex].
- [25] P. Ferrario and G. Rodrigo, JHEP **1002**, 051 (2010) [arXiv:0912.0687 [hep-ph]].
- [26] F. Halzen, P. Hoyer and C. S. Kim, Phys. Lett. B **195**, 74 (1987).
- [27] J. A. Aguilar-Saavedra, A. Juste and F. Rubbo, Phys. Lett. B **707**, 92 (2012) [arXiv:1109.3710 [hep-ph]].
- [28] [Tevatron Electroweak Working Group and CDF and D0 Collaborations], arXiv:1107.5255 [hep-ex].
- [29] J. Pumplin, D. R. Stump, J. Huston, H. L. Lai, P. M. Nadolsky and W. K. Tung, JHEP **0207**, 012 (2002) [hep-ph/0201195].
- [30] T. Hahn, Comput. Phys. Commun. **168**, 78 (2005) [hep-ph/0404043].
- [31] M. Galassi *et al.*, GNU Scientific Library Reference Manual (3rd ed.), ISBN 0954612078, <http://www.gnu.org/software/gsl/>.
- [32] T. Aaltonen *et al.* [CDF Collaboration], CDF Public Note 9850 (2009).
- [33] P. H. Frampton and S. L. Glashow, Phys. Lett. B **190**, 157 (1987).

- [34] C. T. Hill, Phys. Lett. B **266**, 419 (1991).
- [35] R. S. Chivukula, A. Farzinia, E. H. Simmons and R. Foadi, Phys. Rev. D **85**, 054005 (2012) [arXiv:1111.7261 [hep-ph]].
- [36] B. Lillie, L. Randall and L. -T. Wang, JHEP **0709**, 074 (2007) [hep-ph/0701166].
- [37] J. H. Kühn and G. Rodrigo, Phys. Rev. D **59**, 054017 (1999) [hep-ph/9807420].
- [38] G. Aad *et al.* [ATLAS Collaboration], ATLAS-CONF-2012-088.
- [39] S. Chatrchyan *et al.* [CMS Collaboration], CMS-PAS-EXO-12-016.
- [40] U. Haisch and S. Westhoff, JHEP **1108**, 088 (2011) [arXiv:1106.0529 [hep-ph]].
Update: S. Westhoff, talk given at Planck 2012, Warsaw.
- [41] P. H. Frampton, J. Shu and K. Wang, Phys. Lett. B **683**, 294 (2010) [arXiv:0911.2955 [hep-ph]].
- [42] T. Aaltonen *et al.* [CDF Collaboration], Phys. Rev. Lett. **102**, 222003 (2009) [arXiv:0903.2850 [hep-ex]].
- [43] G. Aad *et al.* [ATLAS Collaboration], arXiv:1207.5644 [hep-ex].
- [44] S. Chatrchyan *et al.* [CMS Collaboration], CMS-PAS-TOP-12-013.
- [45] G. M. Tavares and M. Schmaltz, Phys. Rev. D **84**, 054008 (2011) [arXiv:1107.0978 [hep-ph]].